Production of lightning NO_x and its vertical distribution calculated from 3-D cloud-scale chemical transport model simulations

Lesley Ott, UMBC/GEST, Greenbelt, MD

Kenneth Pickering, NASA Goddard Space Flight Center, Greenbelt, MD

Georgiy Stenchikov, Rutgers University, New Brunswick, NJ

Dale Allen, University of Maryland, College Park, MD

Alex DeCaria, Millersville University, Millersville, PA

Brian Ridley, National Center for Atmospheric Research, Boulder, CO

Ruei-Fong Lin, UMBC/GEST, Greenbelt, MD

Steve Lang, SSAI, Greenbelt, MD

Wei-Kuo Tao, NASA Goddard Space Flight Center, Greenbelt, MD

For submission to *Journal of Geophysical Research*

February 9, 2009

Abstract

A 3-D cloud scale chemical transport model that includes a parameterized source of lightning NO_x based on observed flash rates has been used to simulate six midlatitude and subtropical thunderstorms observed during four field projects. Production per intracloud (P_{IC}) and cloud-to-ground (P_{CG}) flash is estimated by assuming various values of P_{IC} and P_{CG} for each storm and determining which production scenario yields NO_x mixing ratios that compare most favorably with in-cloud aircraft observations. We obtain a mean P_{CG} value of 500 moles NO (7 kg N) per flash. The results of this analysis also suggest that on average, P_{IC} may be nearly equal to P_{CG}, which is contrary to the common assumption that intracloud flashes are significantly less productive of NO than are cloud-to-ground flashes. This study also presents vertical profiles of the mass of lightning NO_x after convection based on 3-D cloud-scale model simulations. The results suggest that following convection, a large percentage of lightning NO_x remains in the middle and upper troposphere where it originated, while only a small percentage is found near the surface. The results of this work differ from profiles calculated from 2-D cloud-scale model simulations with a simpler lightning parameterization that were peaked near the surface and in the upper troposphere (referred to as a "C-shaped" profile). The new model results (a backward C-shaped profile) suggest that chemical transport models that assume a C-shaped vertical profile of lightning NO_x mass may place too much mass near the surface and too little in the middle troposphere.

1. Introduction

The oxides of nitrogen, ($NO + NO_2 = NO_x$), are important O_3 precursors in the troposphere. Of the major sources of NO_x in the troposphere, lightning remains the source with the greatest uncertainty and is particularly important because it produces NO_x in the middle and upper troposphere where NO_x is longer lived and can be more efficient at producing ozone than in the boundary layer. The representation of lightning NO_x (LNO_x) in three-dimensional (3-D) regional and global chemical transport models (CTMs) is critical to the models' representation of ozone and other species such as OH [e.g. Stockwell et al., 1999, Labrador et al., 2004]. Labrador et al. [2005] found that both the magnitude of the global LNO_x source strength and its vertical distribution can substantitally affect tropospheric trace gas concentrations in a global CTM. IPCC [2007] suggests a global LNO_x source of 1.1-6.4 Tg N yr^{-1} based on the work of Boersma et al. [2005]. However, Schumann and Huntrieser et al. [2007] have comprehensively summarized estimates of global LNO_x production and found the best estimate to be 5±3 Tg N yr^{-1}.

In order to adequately represent the LNO_x source in global or regional models, the geographic distribution of flashes, average production of NO per flash, and vertical distribution of LNO_x following convection must be specified. A variety of schemes have been used to specify the horizontal distribution of flashes (e.g. using variables such as cloud-top height, upward cloud mass flux, convective preciptation, and CAPE as predictors). Allen and Pickering [2002] have evaluated their use in global 3-D CTMs. The production of NO per flash has also been examined using laboratory experiments, theoretical assumptions regarding the physics of lightning flashes, and observations obtained during field projects. Despite these efforts, a great deal of uncertainty remains

73 regarding NO production on a per flash basis, as well as the relative production by
74 intracloud (IC) and cloud-to-ground (CG) flashes. On the basis of previous studies,
75 which suggested that IC flashes were less energetic than CG flashes (e.g. Holmes et al..
76 1971), many studies of lightning NO_x production have assumed that P_{IC} is less than P_{CG}.
77 Price et al. [1997] assumed that a CG flash produces approximately 1100 moles of NO
78 and that an IC flash was one tenth as productive of NO as a CG flash in estimating global
79 lightning NO_x production.
80 However, a number of more recent studies have suggested that P_{IC} may be nearly
81 as great as P_{CG}. Gallardo and Cooray [1996] suggested that IC flashes may dissipate
82 nearly as much energy as CG flashes and therefore P_{IC} may be on the order of P_{CG}.
83 Supporting the Gallardo and Cooray [1996] hypothesis, a two-dimensional (2-D) cloud-
84 scale modeling study by DeCaria et al. [2000] suggested that the P_{IC}/P_{CG} ratio is likely
85 between 0.5 and 1.0 and a 3-D modeling analysis by DeCaria et al. [2005] narrowed this
86 range to between 0.75 and 1.0. A study by Fehr et al. [2004] used a 3-D cloud-scale
87 model simulation of a storm observed over Germany, and by comparing with lightning
88 and aircraft observations, concluded that on average, an IC flash produced 40% more NO
89 than a CG flash. Zhang et al. [2003] argued that IC flashes may dissipate 50-100% as
90 much energy as CG flashes because they have a large number of return strokes which
91 where neglected in the Price et al. [1997) calculations. Rahman et al. [2007] found that
92 results from experiments with rocket-triggered lightning suggested that NO_x production
93 was associated with relatively long duration continuing currents, which may be greater in
94 IC flashes than in CG flashes, leading to the implication that IC flashes may produce as
95 much or possibly more NO_x per flash than CG flashes. Recent estimates of energy
96 dissipated by IC and CG flashes using electrical potential and charge density

97 measurements by Maggio et al. [2008] also suggest IC flashes may dissipate as much or
98 more energy than CG flashes.

99 Pickering et al. [1998] presented vertical profiles of lightning NO_x for use in 3-D
100 CTMs based on the results of 2-D cloud-resolving model simulations of seven convective
101 events. These simulations assumed the production scheme of Price et al. [1997]. NO_x
102 produced by CG flashes was distributed in the simulated storms from the surface to the -
103 15°C isotherm while NO_x produced by IC flashes was distributed from the -15°C
104 isotherm to the cloud top. Average profiles of LNO_x mass computed for the midlatitude
105 continental, tropical continental, and tropical marine regimes showed peaks in mass near
106 the surface and in the upper troposphere, leading many CTMs to adopt a C-shaped
107 vertical distribution of LNO_x mass.

108 This paper has two primary objectives: (1) to summarize the results of 3-D cloud-
109 resolved storm simulations yielding estimates of NO production per flash and (2) to
110 update the vertical LNO_x profile information of Pickering et al. [1998]. Six storms from
111 field projects conducted in Germany, Colorado, south Florida, and Kansas/Oklahoma
112 have been simulated using a 3-D cloud-scale chemical transport model (CSCTM) that
113 includes a parameterized source of LNO_x. LNO_x production per flash is estimated
114 individually for five of the six storms. In this study we present vertical distributions of
115 LNO_x calculated from each of these 3-D simulations as well as average vertical profiles
116 for the midlatitude continental and subtropical events, which can be applied in regional
117 and global CTMs. Section 2 describes the methodology used in these studies, while
118 section 3 presents results from the individual storm simulations. Section 4 discusses the
119 results of the storm case studies and their application to global models and remote
120 sensing. Section 5 presents conclusions that may be drawn from this work.

2. Methodology

Storms from the Cirrus Regional Study of Tropical Anvils and Cirrus Layers – Florida Area Cirrus Experiment (CRYSTAL-FACE; Ridley et al., 2004; Lopez et al., 2006), European Lightning Nitrogen Oxides Project (EULINOX; Huntrieser et al, 2002), Stratosphere Troposphere Experiment: Radiation, Aerosols and Ozone (STERAO; Dye et al., 2000), and Preliminary Regional Experiment for STORM (PRE-STORM; Rutledge and MacGorman, 1988) field projects were simulated. With the exception of the PRE-STORM event, all of these storms featured measurements of chemical and meteorological properties by research aircraft at anvil levels. The time, location, and peak current of CG lightning occurrences in all storms were recorded by ground-based systems, and during STERAO and EULINOX, total lightning activity (IC + CG) was mapped by a VHF interferometer. In addition, all experiments included extensive satellite and radar observations of storm development and evolution.

The dynamical evolution of each storm was simulated using a cloud-resolving model and the temperature, wind, and hydrometeor fields were then used to drive the offline CSCTM. For each storm, various LNO_x production per flash scenarios were simulated and model results were compared with in-cloud aircraft observations of NO_x through use of mean profiles, column NO_x mass, and probability distribution functions of simulated and observed NO_x to determine the most appropriate scenario. At the end of the CSCTM simulation, the mass of N fixed by lightning was calculated at each model level, and the percentage of the total mass of LNO_x was calculated for 1-km layers.

A detailed description of the CSCTM is found in DeCaria et al. [2005]. In this version of the model, LNO_x production is computed using observed IC and CG flash rates and a specified scenario of P_{IC} and P_{CG} to calculate the mass of NO injected into the

145 cloud per time step. Both laboratory experiments (Wang et al., 1998) and theoretical
146 considerations (Price et al., 1997) have pointed to a strong dependence of LNO_x
147 production on stroke peak current. Therefore, we have made initial estimates of P_{CG}
148 using these relationships because peak current data for return strokes are available from
149 ground-based network observations of CG flashes. However, this assumption contributes
150 to uncertainty in the results because recent work with rocket-triggered lightning (Rahman
151 et al., 2007) has suggested that return strokes are not the primary NO-producing phase of
152 a lightning flash. Field experimental results from TROCCINOX (Tropical Convection,
153 Cirrus and Nitrogen Oxides Experiment) in Brazil (Huntrieser et al., 2008) have
154 suggested a more minor dependence on stroke peak current.
155 The NO produced by CG flashes is distributed unimodally in the vertical, while
156 the NO produced by IC flashes is distributed bimodally based on the vertical distributions
157 of very high frequency (VHF) sources of IC and CG flashes presented in MacGorman
158 and Rust [1998]. The two modes correspond to the two main charge centers in a typical
159 thunderstorm cloud. The vertical distributions of IC and CG lightning channels used in
160 the model are shown in Figure 2 of DeCaria et al. [2005]. The modes of the IC
161 distribution are nominally set at the heights of the -15°C and -45°C isotherms. However,
162 the vertical distribution of IC channels is modified as necessary in some storms by
163 changing the upper mode isotherm to account for a higher or lower cloud top and to
164 match the upper tropospheric peak in aircraft observations of NO_x. At each model level,
165 the lightning NO is distributed uniformly to all grid cells within the 20 dBZ contour
166 computed from simulated hydrometeor fields. A passive version of the CSCTM includes
167 only the transport of tracer species and production of lightning NO_x. In this version,
168 three types of NO_x (pre-existing NO_x, CG LNO_x, and IC LNO_x) are transported without

any chemical reactions and the results are used to estimate average NO_x produced by IC and CG flashes. Various production scenarios are specified and the model results compared with in-cloud aircraft observations to determine a first estimate of the most appropriate LNO_x production scenario for the storm in question.

A version of the model that includes O_3 photochemistry is used to separate NO_x into NO and NO_2 and obtain a final and best estimate of NO production by IC and CG flashes. The chemical mechanism for the STERAO storms is described in DeCaria et al. [2005]. In the CRYSTAL-FACE and EULINOX simulations, the chemical scheme is identical to that described in DeCaria et al. [2005] with the exception that in these cases, isoprene and propene chemistry was included. Initial profiles of ozone were constructed using out-of-cloud aircraft observations, and when necessary to fill gaps, climatological ozone profiles appropriate for the latitude of the storm in question. The CSCTM includes a simple scheme to represent the influence of clouds on photolysis rates based on the work of Madronich [1987] and fully described in DeCaria et al. [2005]. Clear sky photolysis rates are calculated following Stamnes et al. [1988] using observed column ozone amounts measured by the Total Ozone Mapping Spectrometer (TOMS) or, in the case of the STERAO storms, ozonesondes launched from Boulder, Colorado. Perturbations to clear sky photolysis rates are determined by cloud thickness with very thick clouds (deeper than 5 km) resulting in photolysis rates multiplied by a factor of 2 above the cloud and 0.1 below the cloud base with a linearly interpolated degree of enhancement at intermediate altitudes.

3. Results

3.1 Subtropical Events

192 The CRYSTAL-FACE experiment was conducted over South Florida in July,
193 2002 and two storms investigated during the campaign were simulated. The July 29
194 CRYSTAL-FACE storm was simulated using the NASA Goddard version of the non-
195 hydrostatic PSU/NCAR (MM5) mesoscale model (Tao et al., 2003b) with a horizontal
196 resolution of 2 km and vertical resolution of 0.5 km. At 1700 UTC (1300 LT) on July 29,
197 2002, a powerful thunderstorm developed along the west coast of Florida near Fort
198 Myers. While the storm intensified and moved north along the coast, the area in and
199 above the anvil was sampled by the NASA WB-57 research aircraft from 1845 to 2011
200 UTC at altitudes ranging from 12.5 to 13.8 km. The coastal convection later merged with
201 convection originating near Lake Okeechobee. Figure 1 shows the time series of CG
202 flashes recorded by the National Lightning Detection Network (NLDN) from 1700 to
203 2300 UTC. The July 29 storm was an exceptionally strong lightning producer with 4168
204 CG flashes recorded during this period. Maximum CG flash rates exceed 30 flashes per
205 minute. These lightning flash rates and their relationship to NO observations from the
206 WB-57 aircraft have been discussed by Ridley et al. [2004].
207 Simulated convection along the coast began earlier than observed by
208 approximately three hours, but a number of storm features were successfully reproduced,
209 including cloud top height and the direction of storm movement. The transport of CO
210 (initial boundary layer maximum) and O_3 (initial stratospheric maximum) were calculated
211 by the CSCTM and compared with in-cloud observations using probability distribution
212 functions (pdfs). The model overestimated the frequency of values in the upper end of
213 the frequency distributions for both CO and O_3 at anvil levels, suggesting that both
214 upward and downward transport in the model may be too strong. However, the intense
215 lightning activity in the thunderstorm and extremely elevated NO_x mixing ratios (up to 10

ppbv) observed in the anvil indicate that the lightning NO_x source in this storm was extremely strong. As a result, errors in transport are unlikely to significantly affect the estimate of LNO_x production per flash in this case.

Because the NLDN only recorded the occurrence of CG flashes during CRYSTAL-FACE, IC flashrates were estimated for the July 29 storm. NLDN flashes with positive peak current less than 10 kA are thought to be IC flashes [Cummins et al., 1998]. These flashes were removed from the NLDN observations to estimate CG flash rates. The percentage of recorded flashes with positive peak current less than 10 kA was calculated during both the July 29 storm and the month of July as a whole. The percentage of such flashes in the July 29 storm was larger by a factor of 2.5 than the percentage for the month of July which may indicate an enhancement of the IC/CG ratio in the July 29 storm over the climatological value. To account for this enhancement, the south Florida climatological value for the IC/CG ratio of 2 from Boccippio et al. [2001] was multiplied by 2.5 to estimate an IC/CG ratio of 5. The upper mode of the vertical distribution of IC flash channel segments was set to -45°C.

P_{CG} was estimated to be approximately 590 moles NO based on observed mean peak current (19 kA) and a relationship between peak current and energy dissipated from Price et al. [1997]. Various values of the P_{IC}/P_{CG} ratio were simulated and the results compared with aircraft NO_x observations (observed NO + estimated NO_2). NO_2 was estimated using NO and O_3 observations and the photostationary state assumption because no direct measurements of NO_2 were available. Following the work of Madronich (1987), who demonstrated that actinic flux and photodissocation could increase within clouds, NO_2 mixing ratios were calculated assuming both clear sky photolysis rates and rates enhanced by a factor of 2. The observed column mass of N in

240 NO_x was calculated for the 1 km thick layer extending from 12.25 to 13.25 km by
241 computing layer mean in-cloud NO_x mixing ratios. Assuming that photolysis rates were
242 enhanced in the cloud yielded a column mass of 6.6×10^{-4} g N m^{-2} while assuming that
243 photolysis rates were unaltered by the cloud yielded a column mass of 7.0×10^{-4} g N m^{-2}.
244 Table 1 shows the sensitivity of CSCTM-calculated column mass to the assumed P_{IC}/P_{CG}
245 ratio. Assuming that an IC flash is on average 60% as productive of NO as a CG flash
246 yields the most favorable comparison with column mass of nitrogen estimated from
247 aircraft observations when an IC/CG ratio of 5 is assumed.

248 Figure 2 shows the pdfs of observed and simulated in-cloud NO_x assuming that
249 P_{IC} equals 50 and 60% of P_{CG} and an IC/CG ratio of 5. When compared with observed
250 pdfs at both 12.5 and 13 km, the production scenario that assumes a P_{IC}/P_{CG} ratio of 0.5
251 compares more favorably than assuming a P_{IC}/P_{CG} ratio of 0.6. The pdfs show that the
252 underestimation of the simulated column mass assuming a P_{IC}/P_{CG} ratio of 0.5 results
253 from the inclusion of gridcells with background NO_x concentrations as well as the
254 underestimation of the distribution at 13 km between 2 and 6 ppbv. Based on the
255 comparison of simulated and observed pdfs and computed column mass, it is estimated
256 that in the July 29 CRYSTAL-FACE storm an IC flash on average produced 50-60% as
257 much NO as a CG flash while an average CG flash produced 590 moles NO. The
258 assumption that an IC flash is one tenth as productive of NO as a CG flash significantly
259 underestimated NO_x when compared to column mass estimates calculated from in-cloud
260 aircraft observations. When chemical reactions were simulated in addition to lightning
261 NO_x production and convective transport, a loss of NO_x occurred due to conversion to
262 reservoir species. The simulated column mass of N in NO_x decreased by approximately
263 5% from the values shown in Table 1. The P_{IC}/P_{CG} ratio of 0.6 was selected for the

subsequent calculations because it continued to provide the best comparison with the column mass estimates derived from aircraft. It should be noted that the production scenario discussed above was deduced assuming that the IC/CG ratio in this particular storm was greater than the climatological IC/CG ratio for south Florida by a factor of 2.5. Because many more weak positive flashes (which are believed to be IC flashes) were recorded in this storm than was typical for the South Florida area during the month of July, it is likely that the IC/CG ratio was elevated above the climatological value. If instead the climatological IC to CG ratio of 2 is assumed, an IC flash must produce 50% more NO than a CG flash to match aircraft observations.

It should be noted that the assumptions of IC/CG ratio, P_{CG} value, and P_{IC}/P_{CG} ratio contribute to uncertainty in the production scenario estimate. Figure 3 shows all the possible production scenarios that yield NO_x mixing ratios which would match observed column mass when IC/CG ratios of 2 or 5 are assumed. The symbols on the curves show our best estimates (P_{CG} = 590 moles/flash with P_{IC}/P_{CG} at 0.6 and 1.5) based on the observed mean peak current. Most literature estimates of P_{CG} range from 200 to 1100 moles NO per flash. For this range of P_{CG} values, the P_{IC}/P_{CG} ratio could range from 0.3 to 4 in the July 29 CRYSTAL-FACE storm. If P_{IC} is assumed to equal P_{CG}, then P_{CG} must be between 350 and 850 moles NO per flash depending on the number of IC flashes which are assumed to have occurred. This analysis puts bounds on the uncertainty associated with assuming a single production scenario. If the IC/CG ratio was known to be 5 for this storm, the uncertainty would be reduced. P_{IC}/P_{CG} would be in the 0.3 to 1.8 range (assuming P_{CG} is between 200 and 1100 moles NO per flash). The assumption that IC and CG lighting are equally productive of NO on a per flash basis would yield a production of 350 moles NO per flash. This analysis demonstrates the need for

288 observations of IC flashes in future experiments and more definitive information on the
289 relationship between peak current or other electrophysical variables and LNO_x
290 production.

291 A vertical cross section of simulated NO_x through the core of the coastal storm at
292 the end of the 240 minute simulation is shown in Figure 4 (assuming P_{CG} = 590 moles
293 NO, P_{IC} = 354 moles NO, and an IC/CG ratio of 5). Maximum NO_x mixing ratios exceed
294 11 ppbv in the convective plume extending west from the Florida coast in the 10 to 12
295 km region. Figure 5 shows the vertical profile of the lightning NO_x mass as it is
296 introduced into the model domain, as well as its profile following convection from the
297 same simulation as Figure 4. The bimodal distribution of the profile of injected LNO_x
298 mass reflects the bimodal distribution of IC flash channel segments calculated by the
299 CSCTM. The upper mode peak is initially smaller in magnitude because the LNO_x is
300 distributed with a dependence on pressure as described in DeCaria et al. [2005]. Upward
301 transport during the storm results in LNO_x originally introduced into the model at
302 altitudes near the lower mode peak residing near the top of the cloud following
303 convection.

304 On July 16, 2002, an isolated convective system developed northwest of Miami
305 shortly after 1900 UTC (1500 LT) and was investigated as part of the CRYSTAL-FACE
306 project. Over the next few hours, the storm moved west across the Florida peninsula and
307 was extensively sampled by the WB-57 from 1936 to 2306 UTC at altitudes ranging from
308 9 to 15.5 km AGL. The storm was simulated using the Advanced Regional Prediction
309 System (ARPS) described in Xue et al. [2000; 2001] with a horizontal resolution of 2 km
310 and vertical resolution varying from 25 m near the surface to 0.5 km near the top of the
311 model domain at approximately 25 km. A number of different types of observations,

312 including radar reflectivity, were assimilated into the simulation. The simulated temporal
313 evolution of the storm matched observations well, as did storm size. The CSCTM was
314 used to calculate the transport of tracer species CO and O_3 and a comparison of model
315 results with anvil aircraft observations showed that the model adequately represented
316 transport within the storm.

317 Figure 6 shows the time series of flash rates recorded by the ground-based NLDN
318 from 1900 to 2300 UTC. In contrast to the July 29 CRYSTAL-FACE storm, the July 16
319 storm was a relatively weak lightning producer with only 301 CG flashes recorded during
320 this period and a maximum CG flash rate of 9 flashes per minute. The percentage of
321 weak positive flashes (peak current < 10kA) was calculated during the July 16 storm and
322 was over 20 times greater during the storm than for the month of July as a whole.
323 Because the flash rate during the storm represented too small a sample to reliably make a
324 large adjustment, IC flash rates were estimated from the observed CG flash rates and the
325 climatological IC to CG ratio of 2 for south Florida from Boccippio et al. [2001]. Based
326 on the mean peak current of CG flashes recorded by the NLDN for this storm (23 kA),
327 P_{CG} was estimated to be 700 moles of NO. In this simulation, the upper mode of the IC
328 flash channel distribution was set to -60°C. Several different values of the P_{IC}/P_{CG} ratio
329 were simulated and the results compared with observations. The assumption that on
330 average, an IC flash produces 75% as much NO as a CG flash yielded the most favorable
331 comparison with the column mass of N in NO_x estimated from observations when
332 chemical reactions were not simulated. The simulation of chemistry led to a decrease in
333 NO_x mixing ratios due to conversion of NO_x to reservoir species such as HNO_3 and PAN.
334 In order to match aircraft observations, a P_{IC}/P_{CG} ratio of 0.9 was needed. Figure 7 shows
335 a vertical cross-section of NO_x calculated assuming this production scenario taken

through the core of the storm after 180 minutes of simulation. Maximum NO_x mixing ratios exceeding 5 ppbv are found at 6.5 km while lower concentrations are found in the upper part of the core and anvil.

Figure 8 shows the percentage of the mass of N in LNO_x in each kilometer-deep layer after both the July 16 and 29 CRYSTAL-FACE storms. Following the July 29 storm, the maximum in the vertical mass distribution is found at anvil levels (~10 – 11 km). In the case of the July 16 storm, the maximum is found in the 6-7 km layer, coincident with the lower mode of the vertical distributions of the LNO_x source in the CSCTM. A smaller peak is found in 9-10 km layer, the height of the upper mode of the distribution, and another peak at 12-13 km, near the top of the cloud. These vertical LNO_x mass distributions are based on the assumed IC to CG ratios of 2 and 5 for the July 16 and 29 storms, respectively. Because IC to CG ratios may be highly variable and were estimated for these simulations, the results of a sensitivity test of the assumption of IC to CG ratios of 2 and 5 are shown for the July 16 storm in Figure 9a and for the July 29 storm in Figure 9b. For both storms, assuming an IC to CG ratio of 2 results in a slightly larger percentage of LNO_x mass residing in the lower and middle portion of the cloud and a smaller percentage of LNO_x mass near the cloud top (12-14 km for the July 16 case and 10-12 km for the July 29 storm).

3.2. Midlatitude Continental Events

The STERAO field project was conducted in June and July, 1996 over northeastern Colorado to study lightning NO_x production and convective transport of chemical species. CG lightning activity was monitored by the NLDN, while total lightning activity, including both CG and IC flashes, was mapped by a VHF interferometer. Two storms observed during the STERAO field project were simulated

360 and lightning NO_x production per flash estimated in each. A similar analysis was
361 conducted for one storm from the EULINOX field project conducted in southern
362 Germany in July 1998. The fourth midlatitude storm simulated was from the 1985
363 PRESTORM experiment conducted over Kansas/Oklahoma.
364 All four midlatitude storms were simulated using the 3-D Goddard Cumulus
365 Ensemble (GCE) model, which is described in Tao and Simpson [1993] and Tao et al.
366 [2003a]. A description of the GCE simulation of the July 12 STERAO storm is contained
367 in Stenchikov et al. [2005], while the results of the chemical transport model simulation
368 are found in DeCaria et al. [2005]. Between 2000 and 2400 UTC (1400 and 1800 LT),
369 188 CG flashes and 2121 IC flashes were recorded by the NLDN and interferometer,
370 respectively. Flash counts for the STERAO storms only include interferometer flashes
371 with duration greater than 100 ms. Whether or not short duration flashes, which would
372 not be recorded by some lightning detection systems, are productive of NO is an open
373 question. DeCaria et al. [2005] estimated that P_{CG} was 460 moles NO based on the mean
374 peak current of 15 kA. Assuming that an IC flash was equally as efficient at producing
375 NO as a CG flash yielded the best comparison with observations in terms of mean
376 vertical profile shapes while a P_{IC}/P_{CG} ratio between 0.75 and 1 compared most favorably
377 with observed column mass.
378 On July 10, 1996, a multi-cellular thunderstorm organized in a northwest to
379 southeast line developed near the Wyoming-Nebraska border at approximately 2100 UTC
380 (1500 LT) and was observed as part of the STERAO campaign [Dye et al., 2000;
381 Skamarock et al., 2000; 2003]. Research aircraft investigated the storm from 2237 to
382 0105 UTC. After 0115 UTC, the storm became unicellular with supercell chracteristics.
383 IC lightning activity dominated throughout the lifetime of the storm with only 77 CG

384 flashes and 3223 IC flashes recorded between 2201 and 0206 UTC. The University of
385 North Dakota Citation aircraft observed maximum NO mixing ratios of 1 ppbv
386 approximately 60 km downstream of the storm cores [Dye et al., 2000].
387 The GCE model with a horizontal resolution of 2 km and 0.5 km vertical
388 resolution was used to simulate the July 10 STERAO storm. The GCE and CSCTM
389 simulations were included in a cloud-chemistry model intercomparison study described in
390 Barth et al. [2007]. Both the magnitude and height of the simulated peak updraft velocity
391 compared well with observations. Convective transport was evaluated by comparing
392 simulated CO and O_3 mixing ratios with observations obtained during two across-anvil
393 transects. While the simulation underrepresented transport during the first transect,
394 mixing ratios in the later transect were reproduced well by the CSCTM simulation,
395 indicating that convective transport was adequate after an initial spin-up period.
396 Simulated storm speed and cloud top heights compared favorably with radar
397 observations. For the simulations of the July 10 STERAO and July 21 EULINOX
398 storms, the parameterization of LNO_x production was modified to simulate individual
399 flashes. The method is fully illustrated in Ott et al. [2007]. Each flash is simulated by
400 selecting grid cells at random from an area of the domain centered just downwind of the
401 maximum updraft, which is similar in size to the area where lightning flashes typically
402 occurred. The downwind location was chosen based on plots of radar reflectivity and
403 flash location in Höller et al. [2000] and Dye et al. [2000] that show the majority of
404 lightning activity occurring slightly downwind of the core updraft region. The number of
405 grid cells included in a flash at each level is determined by vertical distributions adapted
406 from the Gaussian distributions calculated in the original bulk method of LNO_x
407 parameterization described in DeCaria et al. [2005]. Simulations of both the July 10

408 STERAO and July 21 EULINOX storms using both the original and modified LNO_x
409 parameterizations show that the difference in parameterization produces little change in
410 the vertical distribution of LNO_x following convection. The upper mode of the IC flash
411 channel distribution was set to -50°C for the July 10 STERAO storm.
412 In the July 10 STERAO storm, P_{CG} was estimated to be approximately 390 moles
413 based on the observed peak current (13 kA) of CG flashes. Assuming a P_{IC}/P_{CG} ratio of
414 0.5 matched in-cloud aircraft observations well when chemical reactions were not
415 considered. When chemical reactions were simulated, the P_{IC}/P_{CG} ratio was increased to
416 0.6 to match observations. Figure 10 shows a vertical cross section of calculated NO_x
417 through the core of the southernmost cell in the line of thunderstorms at the end of the
418 180 minute simulation. NO_x mixing ratios exceed 2.8 ppbv at 3.5 km above the surface
419 but are only ~1 ppbv in the anvil region.
420 The EULINOX field project was conducted in central Europe in June and July
421 1998 in order to study lightning NO_x production over Europe. In addition to two research
422 aircraft, the project included observations of CG lightning activity from the ground-based
423 lightning detection system known as BLIDS (Blitz Informationsdienst von Siemens).
424 One storm from the EULINOX project, which occurred on July 21, 1998 over southern
425 Germany, was simulated using the GCE model. The storm developed as a single cell and
426 after an initial period of intensification split into two distinct cells. The northernmost cell
427 became multicellular in structure and was observed to decay rapidly, while the southern
428 cell strengthened and developed supercell characteristics. The southern cell produced
429 360 CG and 2565 IC flashes between 1640 and 1900 UTC (1840 and 2100 LT), while the
430 northern storm produced 289 CG and 815 IC flashes. The GCE simulation succeeded in
431 reproducing a number observed storm features, including the cell-splitting. A full

description of the GCE and CSCTM simulations is provided in Ott et al. [2007]. Based on the mean peak current (12 kA) of CG flashes, P_{CG} was estimated to be 360 moles NO. The upper mode of the IC flash channel distribution was set to -45°C in this simulation. Several different values of P_{IC} were simulated, and the scenario in which P_{IC} is equal to P_{CG} was found to compare most favorably with observations, though observed column mass was underestimated by 10%. In order to match observed column mass, the P_{IC}/P_{CG} ratio needed to be increased to 1.15.

In addition to the STERAO and EULINOX storms, the June 10-11 squall line observed during the PRE-STORM project was simulated using the GCE model. The June 10-11 squall line has been documented extensively [e.g. Johnson and Hamilton, 1988; Rutledge et al., 1988] and has previously been simulated using the 2-D version of the GCE [Tao et al., 1993]. In this case, the horizontal resolution of the 3-D GCE was 1.5 km and vertical resolution varied from approximately 0.25 km near the surface to slightly more than 1 km near the top of the domain at 21.4 km. During PRE-STORM, the occurrence of CG lightning flashes was recorded by the National Severe Storms Laboratory's Lightning Location Network. Based on a time series of positive and negative CG flash rates from Nielsen et al. [1994], approximately 6500 CG flashes occurred during the storm's lifetime. Observations of total lightning activity were unavailable, so the climatological IC/CG ratio of 3 for the region [Boccippio et al, 2001] was assumed to estimate IC flash rates. The upper mode of the IC flash channel distribution was set to -45°C. No observations of the chemical environment of the squall line anvil are available. Therefore, it was not possible to estimate a production scenario for IC and CG flashes as in the other five storms. Instead, the average value of P_{CG}

455 calculated over the five other storms (~500 moles NO per flash) was used along with an
456 estimate of P_{IC} that was 85% of P_{CG} or 425 moles of NO.

457 Figure 11 shows the vertical distribution of the mass of N in LNO_x for the four
458 midlatitude continental storms. The distributions for the four storms all reflect the double
459 peaked distribution of LNO_x produced by IC flashes in the model. There is variation
460 between the simulations in the dominant mode of the lightning distributions. In the
461 EULINOX and PRESTORM storms whose IC to CG ratios were on average 5 and 3,
462 respectively, a higher percentage of LNO_x mass is found near the height of the lower
463 mode of the IC distribution, which is also the mode of the CG distribution. In the July 10
464 and July 12 STERAO storms, which had average IC to CG ratios of 33 and 8 during the
465 time periods simulated, a greater percentage of LNO_x mass resides near the height of the
466 upper mode of the IC vertical distribution following convection. In addition to the IC to
467 CG ratio, the dominance of the modes is likely affected by storm dynamics and the
468 timing of IC and CG flashes in relation to the evolution of the storm.

469 4. Applications for large-scale models and remote sensing

470 4.1 Vertical distribution of lightning NO_x mass

471 We have presented results from the simulations of six thunderstorms using the 3-
472 D CSCTM. Figure 12a shows the average vertical distribution of the mass of N in LNO_x
473 calculated by averaging the case studies in the subtropical regime and Figure 12b shows
474 the average vertical distribution for storms in the midlatitude regime overlaid with the
475 vertical distribution calculated by Pickering et al. [1998]. Both plots are overlaid with
476 smooth curves fit to the regime average. Table 2 lists the percentages of LNO_x mass in
477 each 1-km layer taken from the smoothed curves. In both regimes on average, only a
478 small percentage of LNO_x resides in the boundary layer following the convective event.

479 A greater percentage of LNO_x remains in the middle and upper troposphere where the
480 LNO_x was originally produced. These "backward C-shaped" average vertical
481 distributions are in marked contrast to the C-shaped profiles presented in Pickering et al.
482 [1998] based on 2-D cloud-resolving model simulations where a significant percentage of
483 LNO_x mass was transported to the boundary layer and relatively little LNO_x mass was
484 found between 1.5 and 6.5 km after convection concluded. Our results are similar to
485 those from recent 3-D cloud models with explicit electrophysics. For example, Zhang et
486 al. [2003a] found a maximum in NO_x at mid-levels along with a secondary maximum at
487 anvil levels indicating that a large portion of the LNO_x remains within the cloud near the
488 levels of its production. It should also be noted that our simulations indicate a small
489 percentage of mass (~1%) remains above the tropopause following convection, which
490 results from overshooting transport of lightning NO_x produced at lower altitudes.
491 Individual modeling groups who implement these profiles may want to consider scaling
492 these profiles so that mass is not directly injected into the stratosphere because most
493 convective parameterizations used in larger-scale models do not produce overshooting
494 cloud tops. Implementation of the profiles should involve scaling them to calculated
495 cloud top height on an individual grid cell basis.

496 Assuming the density profile of the standard atmosphere, the total mass of
497 lightning NO_x was averaged over the EULINOX and STERAO storms. That amount of
498 NO_x distributed uniformly over a 200 km by 200 km region (typical of a global model
499 grid cell) using the average midlatitude profile shown in Table 2 corresponds to a
500 maximum increase in NO_x mixing ratios of ~ 145 pptv between 7 and 9 km immediately
501 following convection (~2 km higher than the maximum of the lightning NO_x mass
502 distribution). Because the lifetime of NO_x increases with altitude, lightning NO_x will be

503 converted to reservoir species such as PAN and HNO_3 more rapidly in the 7-9 km layer
504 than at higher altitudes. As the time after convection increases, the maximum increase in
505 NO_x mixing ratios due to lightning would be seen at higher altitudes, which is consistent
506 with the C-shaped profile of NO_x typically observed in the troposphere. Downward
507 transport from the stratosphere also contributes to the upper tropospheric maximum in
508 observed NO_x mixing ratios, while the maximum near the surface results from emissions
509 from surface sources such as fossil fuel combustion and soil.

510 The impact of assuming the vertical distributions of lightning NO_x mass presented
511 here has been calculated using NASA's Global Modeling Initiative (GMI) combined
512 stratosphere-troposphere (Combo) CTM. The Combo CTM is detailed in Ziemke et al.
513 [2006] and Duncan et al. [2007]. The tropospheric chemical mechanism includes 80
514 species and 300 reactions to simulate O_3-NO_x-hydrocarbon chemistry [Bey et al. 2001].
515 Lightning is assumed to produce 5 TgN yr^{-1}. Horizontal distribution of lightning NO_x is
516 determined by the locations of parameterized deep convection (as indicated by the upper
517 tropospheric values of cloud mass flux) in the meteorological fields from the Global
518 Modeling and Assimilation Office's GEOS-4 Data Assimilation System that are used to
519 drive the Combo CTM. Flash rates are scaled such that on a regional and monthly basis
520 they match those from the OTD/LIS climatology (Allen et al., 2009).

521 Two one-year simulations were produced by the Combo CTM. The first used the
522 vertical profiles of lightning NO_x from Pickering et al. [1998] while the second
523 simulation used the vertical profiles of lightning NO_x shown in Figure 12a and b for the
524 midlatitude and subtropical regimes. Because no tropical thunderstorms were simulated
525 with the cloud and chemistry models, a hypothetical tropical distribution (Figure 12c)
526 was constructed by extrapolating the subtropical profile to a higher tropopause regime.

527 Test runs of the GMI Combo CTM revealed that this profile performed well in regions
528 dominated by marine convection, but in tropical continental areas the Pickering et al.
529 [1998] profile yielded better results for upper tropospheric ozone compared with
530 ozonesonde data. Therefore, in tropical continental regions the Pickering et al. [1998]
531 profile, modified by removing the boundary layer maximum and redistributing this mass
532 between 4 and 11 km, was used. The tropical profiles are also provided in Table 2.
533 Figure 13 shows the zonal mean change in NO_x and O_3 in January and July when
534 the profiles shown in Figure 12 are used instead of the Pickering et al. [1998] profiles.
535 Because these profiles place less NO in the upper troposphere, NO_x decreases above 10
536 km with decreases over 100 pptv found over the southern hemisphere in January and over
537 the northern hemisphere in July. The decrease in NO_x in the upper troposphere, which
538 results from using the modified vertical profiles of lightning NO_x mass, also causes a
539 small decrease in ozone throughout much of the troposphere. The largest decrease in
540 ozone is ~10 ppbv in July at 15 km and 30°N.
541 4.2. NO production
542 A best-fit production scenario of P_{IC} and P_{CG} has been estimated by comparing in-
543 cloud aircraft observations with model output for the five storms where in-cloud aircraft
544 observations were available. Figure 14 shows the production scenarios estimated for
545 these five storms as well as the production scenario from Price et al. [1997], which was
546 used in calculating the vertical profiles of LNO_x mass presented in Pickering et al. [1998]
547 and has been used in many global CTMs. In all cases, P_{CG} was estimated to be less than
548 the 1100 moles per CG flash given in Price et al. [1997]. In addition, in all cases the ratio
549 of P_{IC} to P_{CG} was greater than the commonly assumed value of 0.1 presented by Price et
550 al. [1997]. Over the five storms simulated, the average estimated P_{CG} was 500 moles NO

551 per flash or 7 kg N per flash (range of 360 to 700 moles per flash or ~5 to 9.8 kg N per
552 flash). Assuming P_{IC}/P_{CG} ratios in the middle of the estimated uncertainty ranges for the
553 July 29 CRYSTAL-FACE, July 12 STERAO, and July 21 EULINOX storms yields an
554 average P_{IC}/P_{CG} ratio of 0.93, corresponding to 465 moles NO. The median peak current
555 (16.5 kA for negative flashes and 19.8 kA for positive flashes, which account for 10.9%
556 of the total) of the North American Lightning Detection Network (NALDN) presented in
557 Orville et al. [2002] corresponds to a P_{CG} value of 508 moles NO when using the Price et
558 al. [1997] relationship between peak current and energy dissipated, which agrees well
559 with our estimate of 500 moles NO per CG flash. Therefore, the cases we have simulated
560 appear to be representative of midlatitude and subtropical lightning. Assuming the
561 average production scenario over the five storms presented, an average global IC to CG
562 ratio of 3 (the same as estimated for the continental United States by Boccippio et al.,
563 2001) , and a global flash rate of 44 flashes s^{-1} [Christian et al., 2003] yields a global
564 lightning NO source of 8.6 Tg N yr^{-1}.

565 Estimates of the global lightning NO source have ranged from 2-20 Tg N yr^{-1}
566 [IPCC, 2001]. This range has been narrowed in recent years. IPCC [2007] recommends
567 a 1.1-6.4 Tg N yr^{-1} range, though a more comprehensive review has specified the range to
568 be 2-8 Tg N yr^{-1} [Schumann and Huntrieser, 2007]. This review considered all of the
569 methods of estimating LNO_x production: global model estimates constrained by various
570 observations, cloud-resolved modeling studies, aircraft measurements, laboratory
571 experiments, and theoretical estimates. Our estimate of 8.6 Tg N yr^{-1} lies near the upper
572 end of the recently established range of global estimates. It is unlikely that our estimate
573 is larger than values in this range due to the global extrapolation. Because of satellite
574 observations of total lightning activity from instruments such as the Optical Transient

575 Detector (OTD; see Christian et al., 2003), uncertainty in the global flashrate has been
576 greatly reduced. Perhaps more likely it is due to the fact that our average production
577 scenario was calculated using data from only midlatitude continental and subtropical
578 storms. No tropical thunderstorms were simulated in this analysis. Because 78% of
579 lightning flashes occur between 30°S and 30°N [Christian et al., 2003], further
580 investigation of the properties of tropical lightning flashes and their production of NO is
581 needed. Based on analysis of data from the TROCCINOX experiment in Brazil,
582 Huntrieser et al. [2008] suggest that tropical flashes (shorter, possibly due to low vertical
583 wind shear) produce less LNO_x than subtropical or midlatitude flashes (longer, possibly
584 due to greater wind shear). If this hypothesis holds true throughout the tropics, inclusion
585 of tropical events into our average production scenario will decrease this average value.
586 Tropical event simulations are currently underway.

587 Several modeling studies have assumed a production scenario similar to the mean
588 scenario presented here where both IC and CG flashes produce on average approximately
589 500 moles NO per flash. Hudman et al. [2007] simulated NO_x over the United States
590 during the ICARTT campaign using the GEOS-Chem CTM and found that assuming a
591 production per flash of 500 moles NO instead of the default GEOS-Chem value of 125
592 moles NO improved the comparison with upper tropospheric aircraft observations.
593 Cooper et al. [2006] simulated LNO_x production and transport over North America
594 during the same period using the FLEXPART model and assumed IC and CG flashes
595 produce 460 moles NO (based on the DeCaria et al. [2005] results for the July 12
596 STERAO storm) and a 2-day lifetime for upper tropospheric NO_x. Resulting ozone
597 enhancements were estimated with a box model. The results showed a good agreement
598 between simulated NO_x and DC-8 aircraft observations and between simulated ozone

599 enhancements and observations from commercial aircraft and ozonesondes. Jourdain et
600 al. [2009] found that assuming a production per flash of 520 moles NO (rather than 260
601 moles NO) in GEOS-Chem simulations of ozone over the United States substantially
602 reduced the model's bias relative to TES observations. Choi et al. [2008] compared
603 results from a regional CTM with tropospheric NO_2 columns from OMI and tropospheric
604 O_3 columns derived from a combination of OMI and MLS data and found that the model,
605 assuming IC and CG flashes produce 500 moles NO, was able to reasonably reproduce
606 the spatial distribution of the satellite observations.

607 4.3 NO_2 in the vicinity of electrified storms

608 NO_2 profiles appropriate for regions dominated by NO_x from lightning are useful
609 for improving satellite retrievals of NO_2 column amounts in such environments. The air
610 mass factor used in converting satellite-measured slant columns to vertical columns of
611 NO_2 is highly dependent on the NO_2 profile shape. NO_2 profiles from the version of the
612 CSCTM that includes chemical production and loss have been used to examine the
613 structure of this species in the CRYSTAL-FACE, STERAO, and EULINOX storms.

614 Mean vertical profiles of NO_2 after convection are shown in Figure 15. The
615 profiles were calculated over a 40 by 40 km area positioned in the convective core region
616 of the model domain. The July 29 profile shows extremely elevated NO_2 mixing ratios
617 exceeding 2 ppbv from 5 to 7.5 km, while the July 16 profile maximizes at only 0.7 ppbv
618 at 9.5 km. The disparity in profiles is due to the large difference in flash rates in the two
619 storms with over 4000 CG flashes recorded by the NLDN in the July 29 storm, and only
620 301 CG flashes recorded in the July 16 storm. Of the midlatitude storms, the vertical
621 profile of NO_2 from the EULINOX storm (with both high flash rate and pollution inflow)

622 is much larger than in either of the STERAO storms with a maximum of nearly 3 ppbv at
623 5.5 km.

624 In addition to NO_2 profiles, we have also used these simulations to estimate
625 partial columns of NO_2 that a satellite may be able to observe in the upper portion of a
626 convective cloud. Vasilkov et al. [2008] compared cloud-top pressures retrieved in the
627 UV wavelengths by the Ozone Monitoring Instrument (OMI) aboard the Aura satellite
628 with those retrieved by IR measurements from MODIS aboard Aqua. A comparison of
629 both cloud-top pressure products with CloudSat radar observations indicate that OMI
630 may be able to measure NO_2 as far down as 400 to 600 mb in the presence of deep
631 convective clouds. Partial NO_2 columns were calculated for our storms of interest by
632 averaging 2-km model output over 13 km by 24 km areas equivalent to OMI's nadir
633 footprint and integrating the column from 400 mb to the tropopause. The results are
634 shown in Figure 16. The July 29 CRYSTAL-FACE and July 21 EULINOX storms show
635 the greatest degree of enhancement, which is consistent with the NO_2 profiles shown in
636 Figure 15. In the July 29 CRYSTAL-FACE storm, the region of highly elevated NO_2
637 columns extends over 100 km. Table 3 shows the sensitivity of the peak and background
638 NO_2 columns to the choice of column depth. The peak values indicate the maximum
639 partial NO_2 column amounts over an OMI grid box area (13 km by 24 km) in the storm
640 anvil or core regions, while the background values indicate the mean partial NO_2 column
641 amounts outside of the storm region. These data should be useful in providing a range of
642 values of tropospheric column NO_2 that may be compared to retrievals over convective
643 clouds from such instruments as OMI.

644 5. Conclusions

645 Simulations of six midlatitude and subtropical thunderstorms occurring during
646 four field projects have been conducted using the CSCTM, which includes a
647 parameterized source of LNO_x. In order to estimate LNO_x production per flash in each
648 storm, different scenarios of P_{IC} and P_{CG} were specified in the model, and the results
649 compared with in-cloud aircraft observations of NO_x. By comparing column mass and
650 probability distribution functions of the observed and simulated storms, the most
651 appropriate production scenario was estimated for each storm. The results suggest that
652 P_{IC} may be nearly the same as P_{CG}. A frequent assumption that P_{IC} is equal to one tenth
653 P_{CG} resulted in a significant underestimation of LNO_x in all five simulations where anvil
654 observations were available. We echo the recommendation of Ridley et al. [2005] for use
655 of comparable values of P_{CG} and P_{IC}. The Ridley et al. [2005] recommendation was
656 partly based on one of the cases presented here. Our similar results for four additional
657 cases strengthen this recommendation. The mean P_{CG} obtained from the five case
658 simulations is 500 moles NO per flash (range 360 to 700), which, when extrapolated
659 globally, yields an estimate at the high end of the currently accepted range. This may
660 result from the absence of tropical flashes in this analysis.
661 Vertical profiles of the percentage of LNO_x mass in each 1-km layer after the
662 convection show very little LNO_x mass near the surface with the majority of LNO_x
663 remaining in the mid- and upper troposphere in a "backward C-shaped" profile. Global
664 and regional CTMs that have adopted C-shaped vertical profiles of LNO_x mass may be
665 underestimating the amount of LNO_x in the mid- troposphere and overestimating the
666 amount near the surface. Global models which are changed to represent equivalent per
667 flash production by IC and CG lightning may require a change of the global LNO_x source
668 strength to reasonably reproduce NO_x observations in the middle and upper troposphere.

Changes in the vertical placement of LNO_x in CTMs may significantly alter distributions of species such as O_3 and OH.

Acknowledgements: The authors would like to acknowledge the contribution of the following individuals who provided observational data: Jimena Lopez and Max Loewenstein from NASA Ames Research Center; Eric Richard from NOAA Earth System Research Laboratory; Jim Dye and Mary Barth from NCAR; Heidi Huntrieser and Hartmut Höller from Deutsches Zentrum für Luft- und Raumfahrt. The authors also wish to thank Donghai Wang, formerly of NASA Langley Research Center, for providing the ARPS simulation of the July 16 CRYSTAL-FACE storm.

References

Allen, D. J., and K. E. Pickering (2002), Evaluation of lightning flash rate parameterizations for use in a global chemical-transport model , *J. Geophys. Res.*, *107*(D23), 4711,doi:10.1029/2002JD002066.

Allen, D. J., K. E. Pickering, J. Rodriguez, B. Duncan, S. Strahan, and M. Damon (2009), Impact of lightning-NO emissions on North American photochemistry as determined using the GMI model, in preparation for *J. Geophys. Res.*

Barth, M. C., S.-W. Kim, C. Wang, K. E. Pickering, L.E. Ott, G. Stenchikov, M. Leriche, S. Cautenet, J.-P. Pinty, C. Barthe, C. Mari, J. H. Helsdon, R. D. Farley, A. M. Fridlind, A. S. Ackerman, V. Spiridonov, and B. Telenta (2007), Cloud-scale model intercomparison of chemical constituent transport in deep convection, *Atmos. Chem. Phys.*, *7*, 4709-4731.

Beirle, S., N. Spichtinger, A. Stohl, K. L. Cummins, T. Turner, D. Boccippio, O. R. Cooper, M. Wenig, M. Grzegorski, U. Platt, and T. Wagner (2006), Estimating the NO_x produced by lightning from GOME and NLDN data: a case study in the Gulf of Mexico, *Atmos. Chem. Phys.*, *6*, 1075-1089.

Bey, I., D. J. Jacob, R. M. Yantosca, J. A. Logan, B. D. Field, A. M. Fiore, Q. Li, H. Y. Liu, L. J. Mickley, and M. G. Schultz (2001), Global modeling of tropospheric chemistry with assimilated meteorology: Model description and evaluation, *J. Geophys. Res.*, *106*(D19), 23,073–23,095.

706 Boccippio, D. J., K. L. Cummins, H. J. Christian, and S. J. Goodman (2001), Combined
707 satellite- and surface-based estimation of the intracloud–cloud-to-ground lightning ratio
708 over the continental United States, *Monthly Weather Review, 129*, 108–122.
709
710 Boersma, K. F., H. J. Eskes, E. W. Meijer, and H. M. Kelder (2005), Estimates of
711 lightning NOx production from GOME satellite observations, *Atmos. Chem. Phys., 5*,
712 2311-2331.
713
714 Christian, H.J., et al. (2003), Global frequency and distribution of lightning as observed
715 from space by the Optical Transient Detector, *J. Geophys. Res., 108*(D1), 4005,
716 doi:10.1029/2002JD002916
717
718 Choi, Y., A. Eldering, G. Osterman, Y. Wang, D. Cunnold, Q. Yang, E. Bucsela, and K.
719 E. Pickering (2008), Lightning and anthropogenic NOx sources over the U.S. and the
720 western North Atlantic Ocean: 1. Impact on tropospheric O_3 from space-borne
721 observations, submitted to *J. Geophys. Res.*
722
723 Cooper, O. R., et al. (2006), Large upper tropospheric ozone enhancements above
724 midlatitude North America during summer: In situ evidence from the IONS and
725 MOZAIC ozone measurement network, *J. Geophys. Res., 111*, D24S05,
726 doi:10.1029/2006JD007306.
727
728 Cummins, K. L., M. J. Murphy, E. A. Bardo, W. L. Hiscox, R. B. Pyle, and A. E. Pifer
729 (1998), A Combined TOA/MDF Technology Upgrade of the U.S. National Lightning
730 Detection Network, *J. Geophys. Res., 103*, 9035-9044.
731
732 DeCaria, A. J., K. E. Pickering, G. L. Stenchikov, J. R. Scala, J. L. Stith, J. E. Dye, B. A.
733 Ridley, and P. Laroche (2000), A cloud-scale model study of lightning-generated NO_x in
734 an individual thunderstorm during STERAO-A, *J. Geophys. Res.*, *105*, 11,601-11,616.
735
736 DeCaria, A. J., K. E. Pickering, G. L. Stenchikov, and L. E. Ott (2005), Lightning-
737 generated NO_x and its impact on tropospheric ozone production: A three-dimensional
738 modeling study of a Stratosphere-Troposphere Experiment: Radiation, Aerosols, and
739 Ozone (STERAO-A) thunderstorm, *J. Geophys. Res., 110,* D14303,
740 doi:10.1029/2004JD005556.
741
742 Duncan, B. N., S. E. Strahan, Y. Yoshida, S. D. Steenrod, and N. Livesey (2007), Model
743 study of the cross-tropopause transport of biomass burning pollution, *Atmos. Chem.*
744 *Phys., 7*, 3713-3736.
745
746 Dye, J. E., et al., (2000), An Overview of the STERAO--Deep Convection Experiment
747 with Results for the 10 July Storm, *J. Geophys. Res.*, *105*, 10,023-10,045.
748
749 Fehr, T., H. Höller, H. Huntrieser, Model study on production and transport of lightning-
750 produced NO_x in a EULINOX supercell storm (2004), *J. Geophys. Res., 109*, D09102,
751 doi:10.1029/2003JD003935.
752

753 Gallardo, L., and V. Cooray (1996), Could cloud-to-cloud discharges be as effective as
754 cloud-to-ground discharges in producing NO_X?, *Tellus*, *48B*, 641-651.
755
756 Höller, H., H. Huntrieser, C. Feigl, C. Théry, P. Laroche, U. Finke, and J. Seltmann
757 (2000), The Severe Storms of 21 July 1998 – Evolution and Implications for NO_X-
758 Production, in *EULINOX – The European Lightning Nitrogen Oxides Experiment*, edited
759 by H. Höller and U. Schumann, *Rep. DLR-FB 2000-28*, pp. 109-128, Deutches Zentrum
760 für Luft- und Raumfahrt, Köln.
761
762 Holmes, C., M. Brook, P. Krehbiel, and R. McRory (1971), On the power spectrum and
763 mechanism of thunder, *J. Geophys. Res., 76,* 2106-2115.
764
765 Hudman, R. C., et al. (2007), Surface and lightning sources of nitrogen oxides over the
766 United States: Magnitudes, chemical evolution, and outflow, *J. Geophys. Res., 112*,
767 D12S05, doi:10.1029/2006JD007912.
768
769 Huntrieser, H., H. Schlager, C. Feigl, and H. Höller (1998), Transport and production of
770 NO_X in electrified thunderstorms: Survey of previous studies and new observations at
771 mid-latitudes, *J. Geophys. Res.,103,* 28,247-28,264.
772
773 Huntrieser, H., et al., (2002), Airborne measurements of NOx, tracer species, and small
774 particles during the European Lightning Nitrogen Oxides Experiment, *J. Geophys. Res.*,
775 *107*(D11), 4113, doi:10.1029/2000JD000209.
776
777 Huntrieser, H., U. Schumann, H. Schlager, H. Höller, A. Giez, H.-D. Betz, D. Brunner,
778 C. Forster, O. Pinto Jr., and R. Calheiros (2008), Lightning activity in Brazilian
779 thunderstorms during TROCCINOX: implications for NOx production, *Atmos. Chem.*
780 *Phys., 8*, 921-953, 2008.
781
782 IPCC (2001), *Climate Change 2001: The Scientific Basis. Contribution of Working*
783 *Group I to the Third Assessment Report of the Intergovernmental Panel on Climate*
784 *Change*. J. T. Houghton et al., Eds., Cambridge University Press, 892 pp.
785
786 IPCC (2007), *Climate Change 2007: Synthesis Report. Contribution of Working Group I*
787 *to the Fourth Assessment Report of the Intergovernmental Panel on Climate Change* S.
788 Solomon et al. (eds.) Cambridge University Press, 996 pp.
789
790 Johnson, R. H., and P. J. Hamilton (1988), The relationship of surface pressure features
791 to the precipitation and airflow structure of an intense midlatitude squall line. *Mon. Wea.*
792 *Rev., 116*, 1444–1472.
793
794 Jourdain, L., S. S. Kulawik, H. M. Worden, K. E. Pickering, J. Worden, and A. M.
795 Thompson, (2009), Lightning NOx emissions over the USA investigated using TES,
796 NLDN, LRLDN, IONS data and the GEOS-Chem model, *Atmos. Chem. Phys. Discuss.*,
797 9, 1123-1155.
798

799 Labrador, L. J., R. von Kuhlmann, and M. G. Lawrence, (2004), Strong sensitivity of the
800 global mean OH concentration and the tropospheric oxidizing efficiency to the source of
801 NOx from lightning, *Geophys. Res. Lett.*, *31*(6), L06102, doi:10.1029/2003GL019,229.
802
803 Labrador, L. J., R. von Kuhlmann, and M. G. Lawrence, (2005), The effects of lightning-
804 produced NOx and its vertical distribution on atmospheric chemistry: sensitivity
805 simulations with MATCH-MPIC, *Atmospheric Chemistry and Physics, 5*, 1815-1834.
806
807 Lee D.S., I. Köhler, E. Grobler, F. Rohrer, R. Sausen, L. Gallardo-Klenner, J. G. J.
808 Olivier, F. J. Dentener, and A. F. Bouwman (1997), Estimations of global NOx emissions
809 and their uncertainties, *Atmospheric Environment, 31*:12, 1735-1749.
810
811 Levy, H. II, W. J. Moxim, and P. Kasibhatla (1996), A global three-dimensional time-
812 dependent lightning source of tropospheric NO_x. *Journal of Geophysical Research,*
813 *101*(D17), 22,911-22,922.
814
815 Lopez, J. P., et al. (2006), CO signatures in subtropical convective clouds and anvils
816 during CRYSTAL-FACE: An analysis of convective transport and entrainment using
817 observations and a cloud-resolving model, *J. Geophys. Res.*, *111*, D09305,
818 doi:10.1029/2005JD006104.
819
820 MacGorman, D. R., and W. D. Rust (1998), *The Electrical Nature of Storms.* Oxford
821 University Press, 422 pp.
822
823 Madronich, S. (1987), Photodissociation in the Atmosphere 1. Actinic Flux and the
824 Effects of Ground Reflections and Clouds, *J. Geophys. Res., 92*(D8), 9740–9752.
825
826 Maggio, C., T. Marshall, and M. Stolzenburg (2008), Energy estimates for lightning
827 flashes, *EOS Trans. AGU*, 89(53) Fall Meeting Suppl., Abstract AE11A-0294.
828
829 Nielsen, K. E., R. A. Maddox, S.V.Vasiloff (1994), The Evolution of Cloud-to-Ground
830 Lightning within a Portion of the 10–11 June 1985 Squall Line, *Monthly Weather*
831 *Review, 122*, 1809-1817.
832
833 Orville, R. E., G. R. Huffines, W. R. Burrows, R. L. Holle, and K. L. Cummins (2002),
834 The North American Lightning Detection Network (NALDN) - First Results: 1998-2000,
835 *Mon. Wea. Rev., 130, 8*, 2098-2109.
836
837 Ott, L. E., K. E. Pickering, G. L. Stenchikov, H. Huntrieser, and U. Schumann (2007),
838 Effects of lightning NOx production during the 21 July European Lightning Nitrogen
839 Oxides Project storm studied with a three-dimensional cloud-scale chemical transport
840 model, *J. Geophys. Res., 112*, D05307, doi:10.1029/2006JD007365.
841
842 Pickering, K. E., Y. Wang, W.-K. Tao, C. Price, and J.-F. Müller (1998), Vertical
843 distributions of lightning NOx for use in regional and global chemical transport models.
844 *J. Geophys. Res.*, *103*, 31,203-31,216.
845

Price, C., J. Penner, and M. Prather, NOx from lightning (1997), 1, Global distributions based on lightning physics, *J. Geophys. Res.*, *102*, 5929-5941.

Rahman, M., V. Cooray, V. A. Rakov, M. A. Uman, P. Liyanage, B. A. DeCarlo, J. Jerauld, and R. C. Olsen III (2007), Measurements of NOX produced by rocket-triggered lightning, *Geophys. Res. Lett.*, *34*, L03816, doi:10.1029/2006GL027956.

Ridley, B., et al. (2004), Florida thunderstorms: A faucet of reactive nitrogen to the upper troposphere, *J. Geophys. Res.*, 109, D17305, doi:10.1029/2004JD004769.

Ridley B., K. Pickering and J. Dye, (2005), Comments on the parameterization of lightning-produced NO in global chemistry-transport models, *Atmos. Environ.*, *39*, 6184-6187.

Rutledge, S. A. and D. R. MacGorman (1988), Cloud-to- ground lightning activity in the 10-11 June 1985 mesoscale convective system observed during the Oklahoma-Kansas PRE-STORM project, *Mon. Wea. Rev.*, *116,* 1393-1408.

Rutledge, S. A., R. A. Houze Jr., M. I. Biggerstaff, and T. Matejka (1988), The Oklahoma–Kansas mesoscale convective system of 10–11 June 1985: Precipitation structure and single-Doppler radar analysis, *Mon. Wea. Rev.*, *116*, 1409–1430.

Schumann, U. and H. Huntrieser (2007), The global lightning-induced nitrogen oxides source, *Atmos. Chem. Phys.*, *7*, 3823-3907.

Skamarock, W. C., et al. (2000), Numerical simulations of the July 10 Stratospheric-Tropospheric Experiment: Radiation, Aerosols, and Ozone/Deep Convection Experiment convective system: Kinematics and transport, *J. Geophys. Res.*, 105(D15), 19,973–19,990.

Skamarock, W. C., J. E. Dye, E. Defer, M. C. Barth, J. L. Stith, B. A. Ridley, and K. Baumann (2003), Observational- and modeling-based budget of lightning-produced NO_x in a continental thunderstorm, *J. Geophys. Res.*, *108*(D10), 4305, doi:10.1029/2002JD002163.

Stamnes, K., S.-C. Tsay, W. Wiscombe, and K. Jayaweera (1988), Numerically stable algorithm for discrete-ordinate method radiative transfer in multiple scattering and emitting layered media, *Appl. Opt.*, *27*, 2502-2509.

Stenchikov, G. L., K. Pickering, A. DeCaria, W.-K. Tao, J. Scala, L. Ott, D. Bartels, and T. Matejka (2005), Simulation of the fine structure of the 12 July 1996 Stratosphere-Troposphere Experiment: Radiation, Aerosols and Ozone (STERAO-A) storm accounting for effects of terrain and interaction with mesoscale flow, *J. Geophys. Res.*, *110,* D14304, doi:10.1029/2004JD005582.

Stockwell, D. Z., C. Giannakopoulos, P.-H. Plantevin, G. D. Carver, M. P. Chipperfield, K. S. Law, J. A. Pyle, D. E. Shallcross and K.-Y. Wang (1999), Modelling NOx from lightning and its impact on global chemical fields, *Atmos. Environ.*, *33*, 4477-4493.

Tao, W.-K., and J. Simpson (1993), Goddard Cumulus Ensemble Model. Part I: Model description, *Terr., Atmos., Oceanic Sci.*, *4*, 35-72.

Tao, W.-K., J. Simpson, D. Baker, S. Braun, M.-D. Chou, B. Ferrier, D. Johnson, A. Khain, S. Lang, B. Lynn, C.-L. Shie, D. Starr, C.-H. Sui, Y. Wang and P. Wetzel (2003a), Microphysics, Radiation and Surface Processes in the Goddard Cumulus Ensemble (GCE) Model, *Meteorology and Atmospheric Physics, 82,* 97-137.

Tao, W.-K., et al. (2003b), Regional-scale modeling at NASA Goddard Space Flight Center, *Research Signpost - Recent Res. Devel. Atmos. Sci., 2,* 1-52.

Vasilkov, A., J. Joiner, R. Spurr, P. K. Bhartia, P. Levelt, and G. Stephens (2008), Evaluation of the OMI cloud pressures derived from rotational Raman scattering by comparisons with other satellite data and radiative transfer simulations, *J. Geophys. Res., 113*, D15S19, doi:10.1029/2007JD008689.

Wang, Y., A. W. DeSilva, G. C. Goldenbaum, and R. R. Dickerson (1998), Nitric oxide production by simulated lightning: Dependence on current, energy, and pressure, J. *Geophys. Res., 103*(D15), 19,149–19,159.

Xue, M., K. K. Droegemeier, and V. Wong (2000), The Advanced Regional Prediction System (ARPS) - A multiscale non-hydrostatic atmospheric simulation and prediction tool. Part I: Model dynamics and verification, *Meteor. Atmos. Physics., 75,* 161-193.

Xue, M., K. K. Droegemeier, V. Wong, A. Shapiro, K. Brewster, F. Carr, D. Weber, Y. Liu, and D.-H. Wong (2001), The Advanced Regional Prediction System (ARPS) - A multiscale non-hydrostatic atmospheric simulation and prediction tool. Part II: Model physics and applications, *Meteor. Atmos. Physics., 76,* 134-165.

Zhang, X., J. H. Helsdon Jr., and R. D. Farley (2003a), Numerical modeling of lightning-produced NO $_x$ using an explicit lightning scheme: 2. Three-dimensional simulation and expanded chemistry, *J. Geophys. Res.*, *108*(D18), 4580, doi:10.1029/2002JD003225.

Zhang , X., J. H. Helsdon Jr., and R.D. Farley (2003b), Numerical modeling of lightning-produced NO_x using an explicit lightning scheme: 1. Two-dimensional simulation as a "proof of concept", *J. Geophys. Res.*, *108*(D18), 4579, doi:10.1029/2002JD003224.

Ziemke, J. R., S. Chandra, B. N. Duncan, L. Froidevaux, P. K. Bhartia, P. F. Levelt, and J. W. Waters (2006), Tropospheric ozone determine from Aura OMI and MLS: Evaluation of measurements and comparison with the Global Modeling Initiative's chemistry transport model, *J. Geophys. Res., 111*(D19), D19303.

937 Table 1. Calculated column mass of N in NO_x in the July 29 CRYSTAL-FACE storm,
938 assuming an IC/CG ratio of 5
939

P_{CG} (moles NO per flash)	P_{IC}/P_{CG} (IC/CG = 5)	P_{IC}/P_{CG} (IC/CG = 2)	Column Mass (g N m^{-2})
590	0.1	0.25	2.3×10^{-4}
590	0.5	1.3	6.0×10^{-4}
590	0.6	1.5	6.9×10^{-4}
590	0.75	1.9	8.3×10^{-4}
590	1.0	2.5	1.0×10^{-3}

940

940 Table 2. Average Profiles of LNO_x Mass in Percent
941

Altitude Range, km	Subtropical	Midlatitude	Tropical Continental	Tropical Marine
0-1	1.0	2.4	0.2	0.6
1-2	2.1	5	0.5	1.5
2-3	3.9	7.4	0.6	2.9
3-4	5.8	9.3	1.4	4.3
4-5	7.7	10.6	2.7	5.4
5-6	9.3	11.4	4	6.7
6-7	10.5	11.5	5	7.7
7-8	11.0	11	6.2	8.5
8-9	11.0	9.9	8.6	9.6
9-10	10.4	8.3	10.3	10.2
10-11	9.2	6.3	11.6	10.5
11-12	7.5	4.2	12.4	10.2
12-13	5.5	2.2	12.7	8.2
13-14	3.4	0.5	12.4	6.5
14-15	1.5	0	7.6	4.5
15-16	0.2	0	3.0	2.2
16-17	0	0	0.8	0.5

942

943
944

945

Table 3. Partial NO_2 columns (10^{14} molecules cm^{-2}) from the tropopause to 400, 500 and 600 mb

	Tropopause to 400 mb		Tropopause to 500 mb		Tropopause to 600 mb	
Storm	Peak	Background	Peak	Background	Peak	Background
July 16 CRY	33	1	48	1	54	2
July 29 CRY	104	3	159	3	223	4
July 10 STE	13	1	21	1	40	1
July 12 STE	21	4	24	5	24	5
July 21 EUL	90	14	140	16	192	17

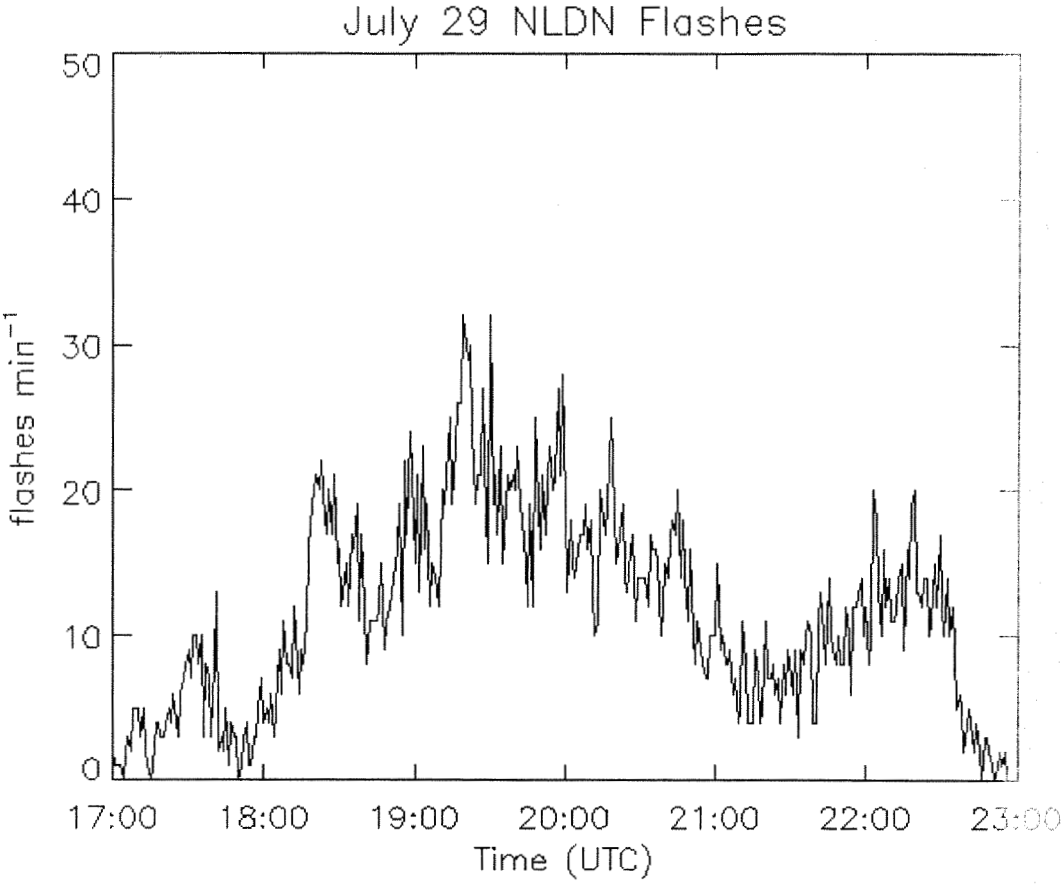

Figure 1. Time series of CG flash rates detected by the NLDN from 1700 to 2300 UTC (1300 and 1900 LT) for the July 29 CRYSTAL-FACE storm.

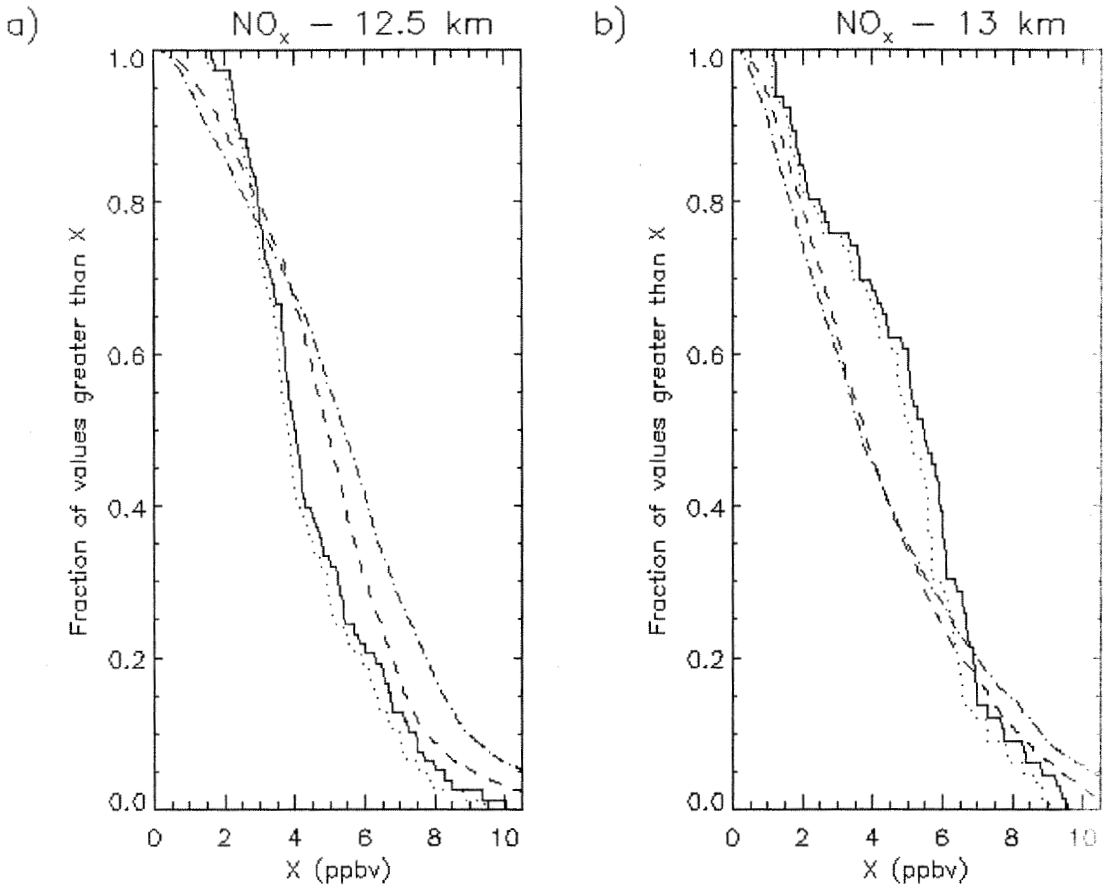

Figure 2. Pdfs of simulated and observed NO_x at 12.5 km (a) and 13 km (b) for the July 29 CRYSTAL-FACE storm. Solid (dashed) line shows observed values assuming clear sky (cloud enhanced) photolysis rates. Dashed (dot-dashed) line shows simulated values assuming P_{IC}/P_{CG} of 0.5 (0.6).

984

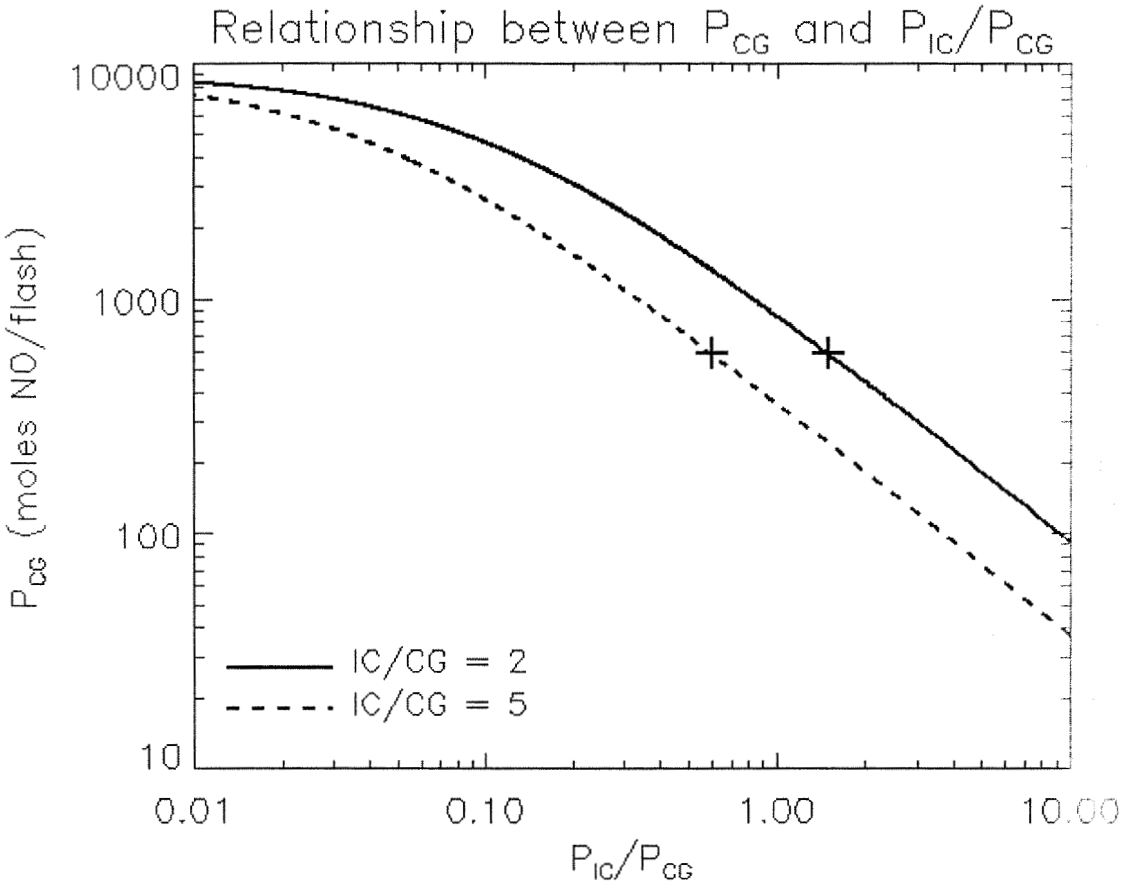

985
986 Figure 3. Relationship between P_{CG} and the P_{IC}/P_{CG} ratio necessary to match the column
987 mass of N computed from aircraft observations. Solid (dashed) line shows the
988 relationship when an IC/CG ratio of 2 (5) is assumed. Plus signs indicate the production
989 scenarios when P_{CG} is assumed to be 590 moles NO per flash based on observed mean
990 peak current.

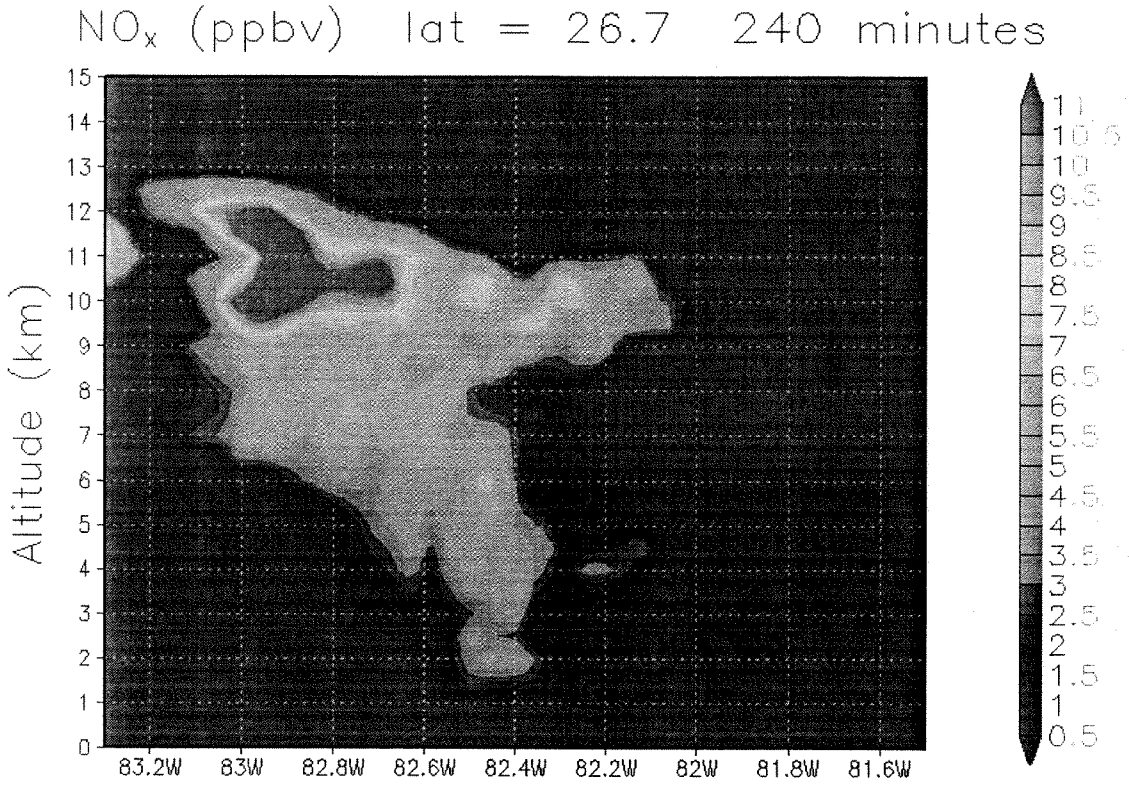

Figure 4. Vertical cross-section of simulated NO_x in the July 29 CRYSTAL-FACE storm (assuming P_{CG} = 590 moles NO, P_{IC} = 354 moles NO, and an IC/CG ratio of 5) at 240 minutes.

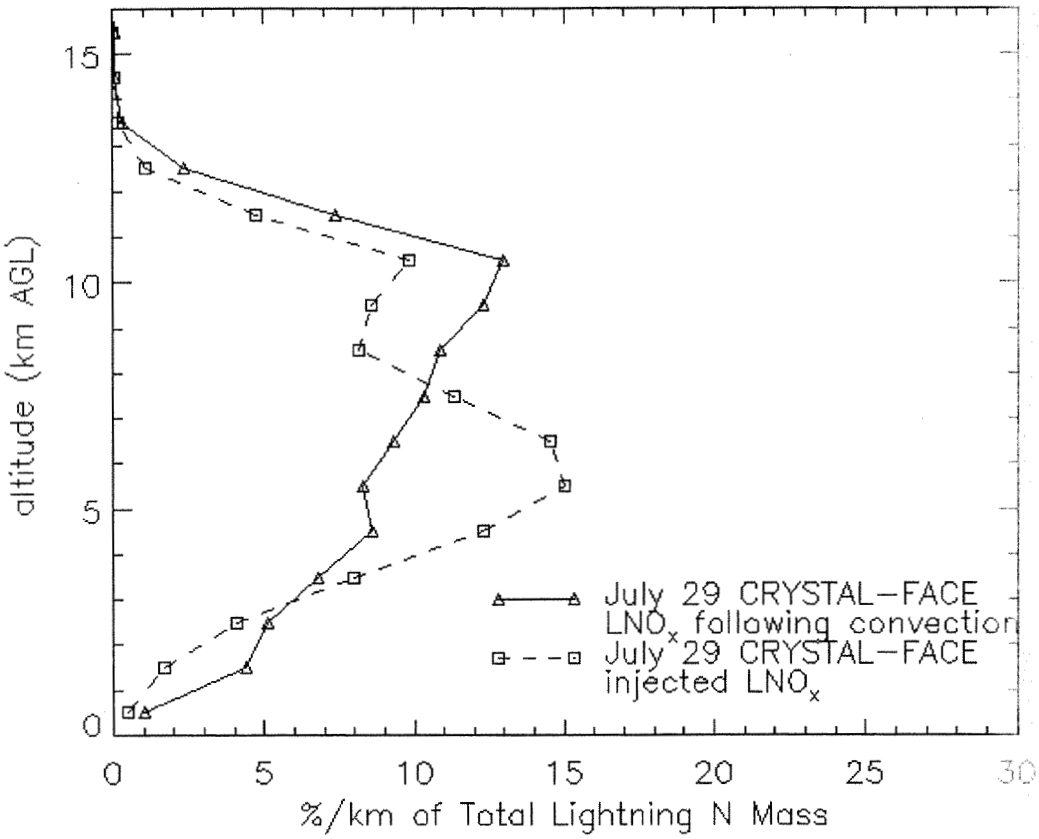

997
998 Figure 5. Vertical distributions of the percentage of LNO_x mass per kilometer injected
999 into the cloud and following convection for the July 29 CRYSTAL-FACE storm
1000 (assuming P_{CG} = 590 moles NO, P_{IC} = 354 moles NO, and an IC/CG ratio of 5).
1001
1002
1003

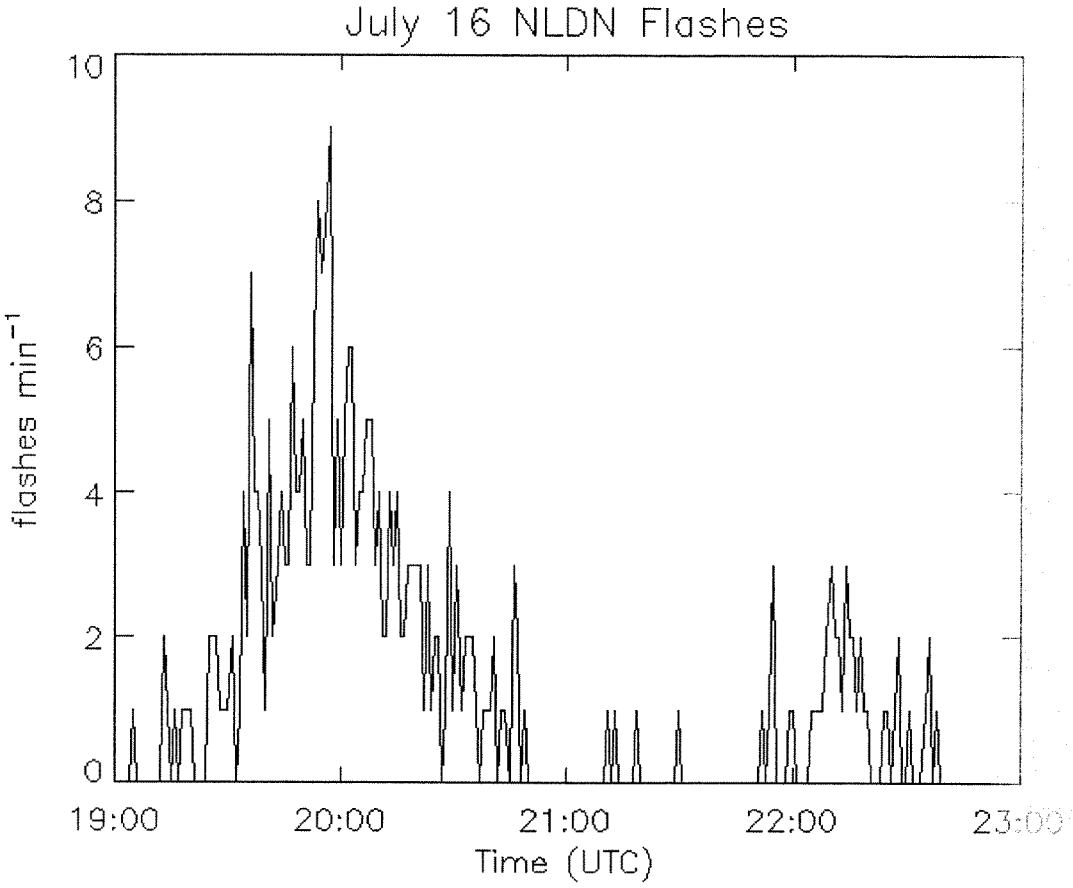

Figure 6. Time series of CG flash rates detected by the NLDN from 1900 to 2300 UTC (1500 to 1900 LT) for the July 16 CRYSTAL-FACE storm.

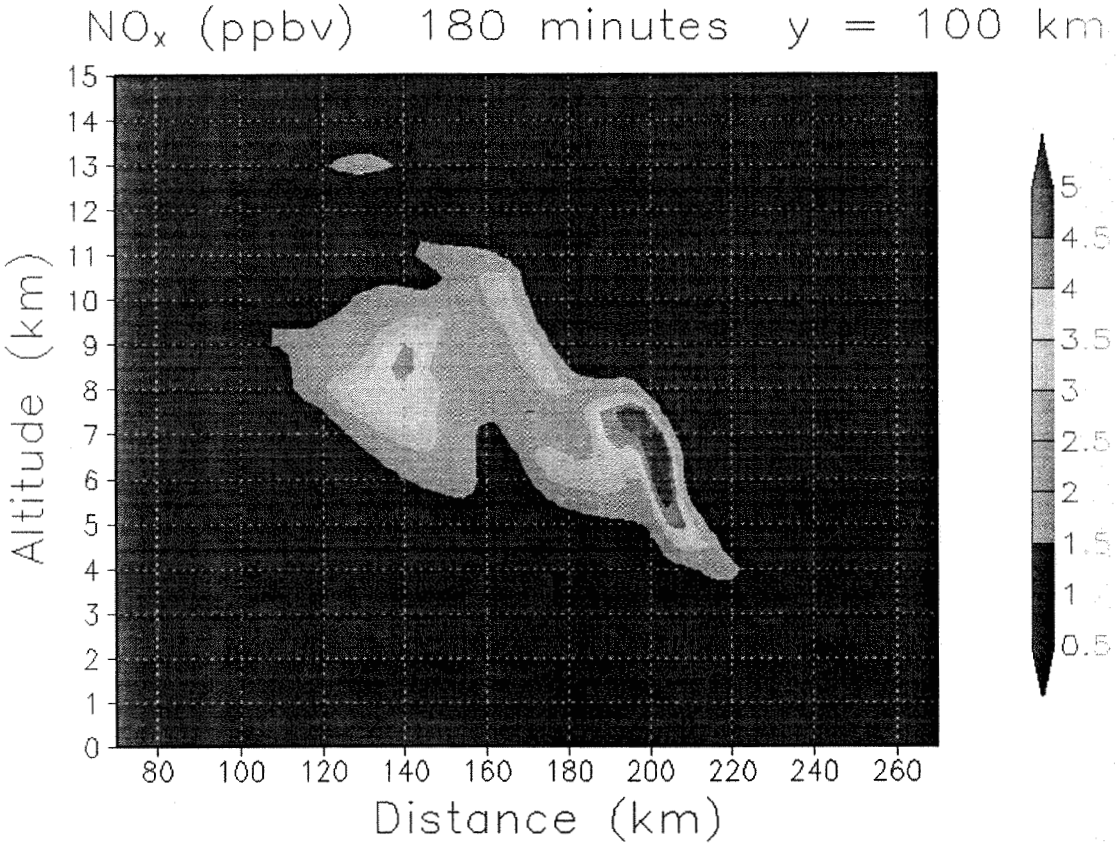

Figure 7. Vertical cross-section of simulated NO_x through the core of the July 16 CRYSTAL-FACE storm assuming P_{CG} = 700 moles NO and P_{IC} = 630 moles NO at 180 minutes.

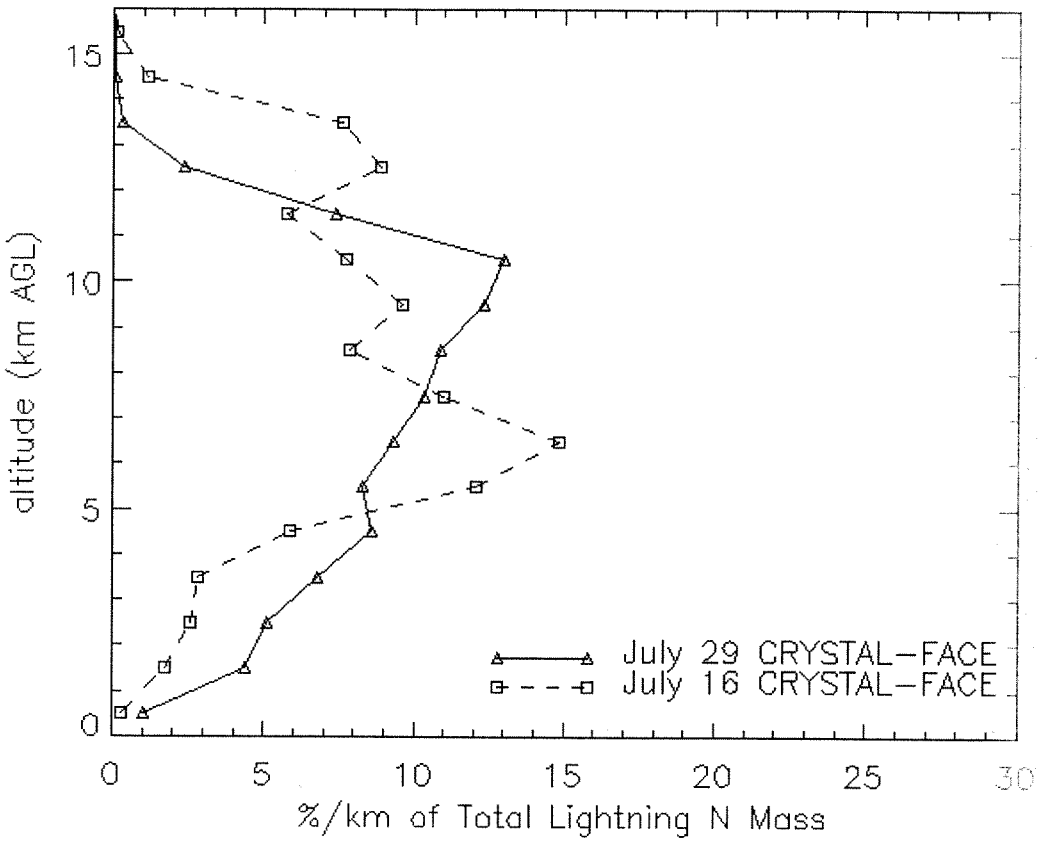

Figure 8. Vertical distributions of percentage of LNO_x mass per kilometer following convection for two simulated subtropical storms.

1019

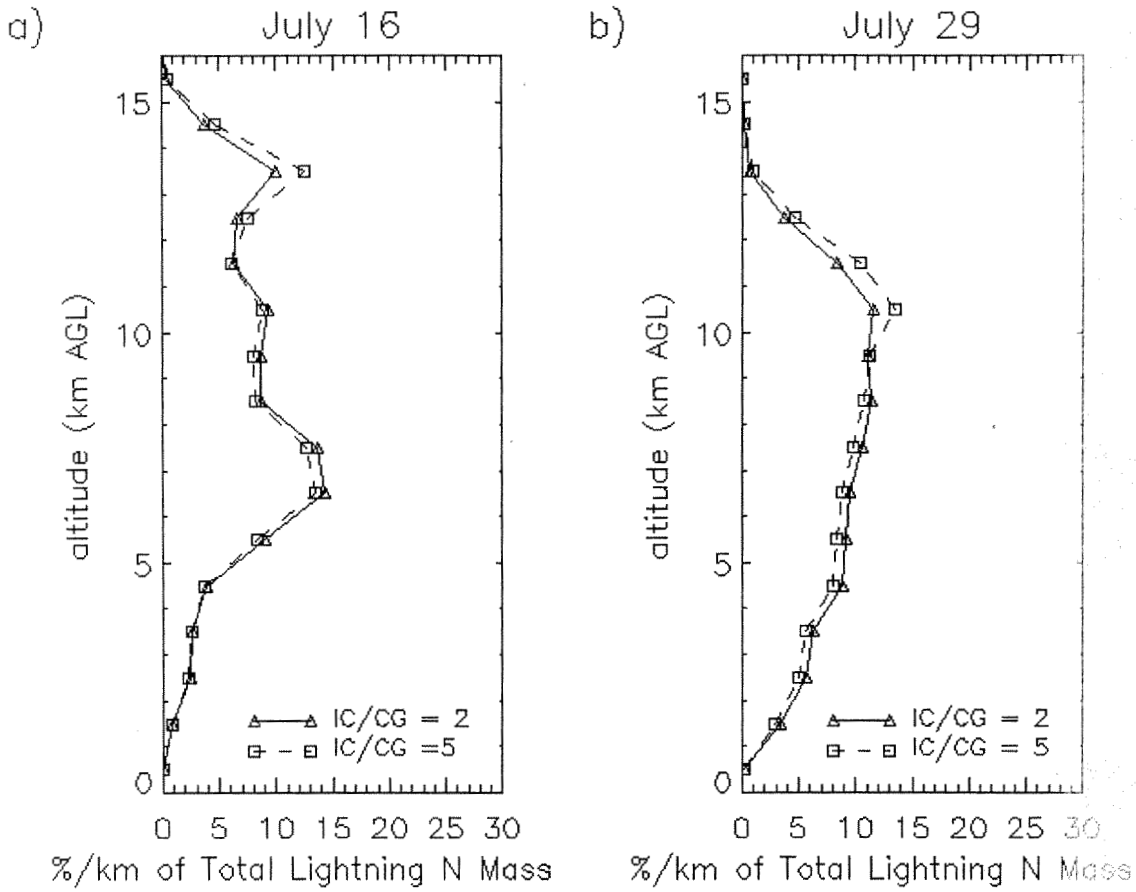

1020
1021

1022 Figure 9. Vertical distributions of the percentage of LNO_x mass per kilometer following
1023 convection for (a) the July 16 and (b) the July 29 CRYSTAL-FACE simulations
1024 assuming IC to CG ratios of 2 and 5.

1025
1026

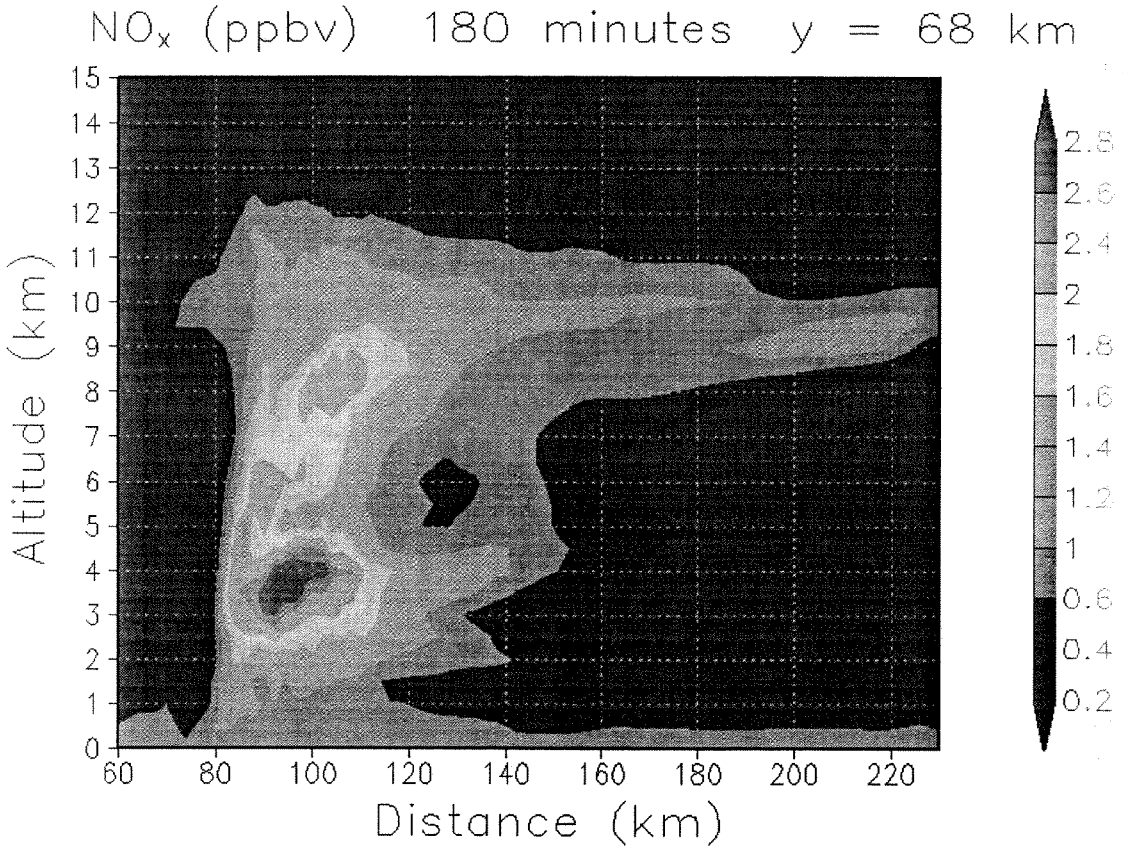

Figure 10. Vertical cross-section of simulated NO_x through the core of the southern cell of the July 10 STERAO storm assuming P_{CG}=390 moles NO and P_{IC}=234 moles NO at 180 minutes.

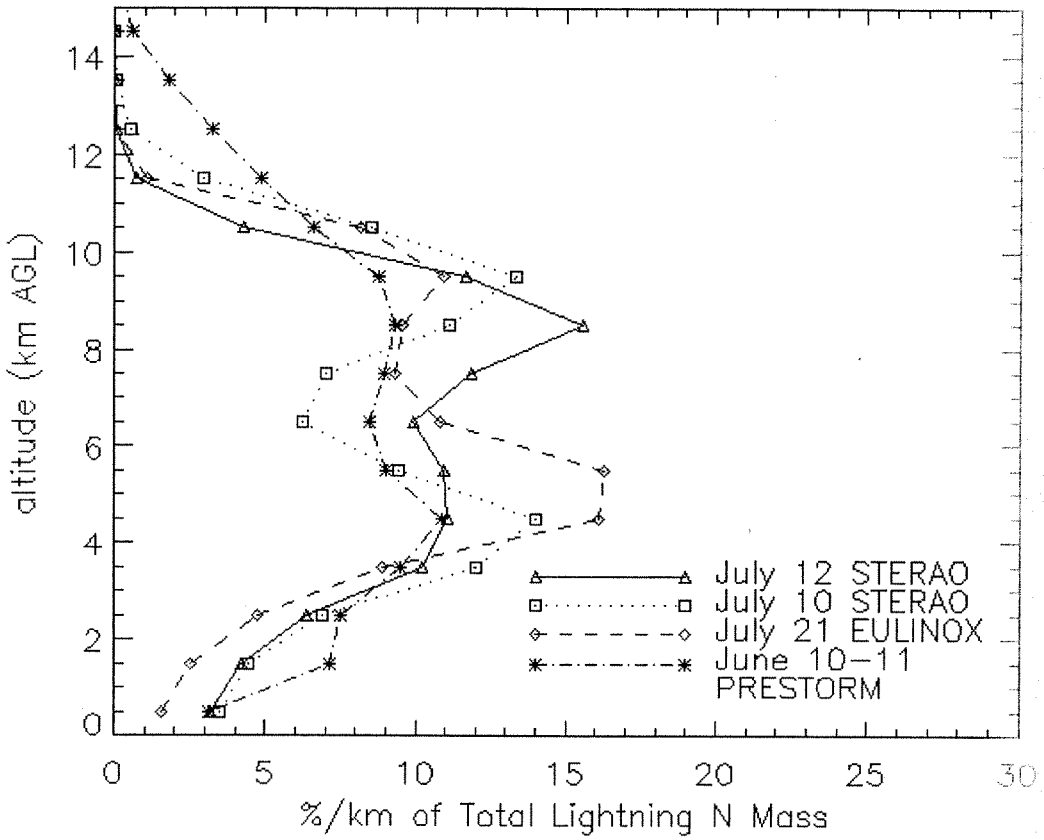

1032
1033
1034 Figure 11. Vertical distributions of percentage of LNO_x mass per kilometer following
1035 convection for four simulated midlatitude continental storms.
1036
1037
1038

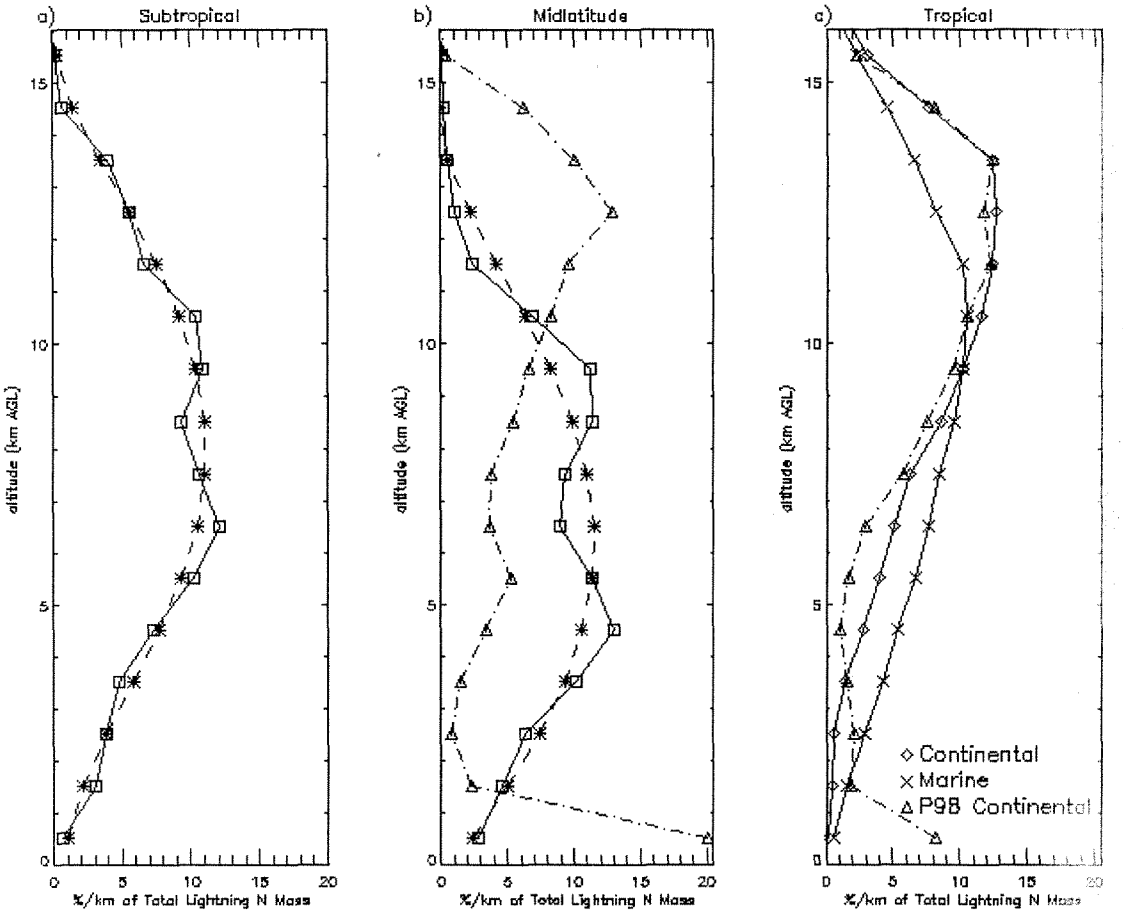

Figure 12. Average vertical distribution of percentage of LNO_x mass per kilometer following convection (solid) for the (a) subtropical and (b) midlatitude continental regimes. Dashed line shows polynomial fit. Midlatitude continental profile from Pickering et al. [1998] (dash-dot) is also shown in (b). Hypothetical tropical marine profile (c) is based on extrapolating the subtropical average profile to a higher tropopause regime while the tropical continental profile was constructed using the Pickering et al. [1998] profile with the boundary layer maximum removed and that mass redistributed into layers from 4 to 11 km.

1049
1050
1051
1052

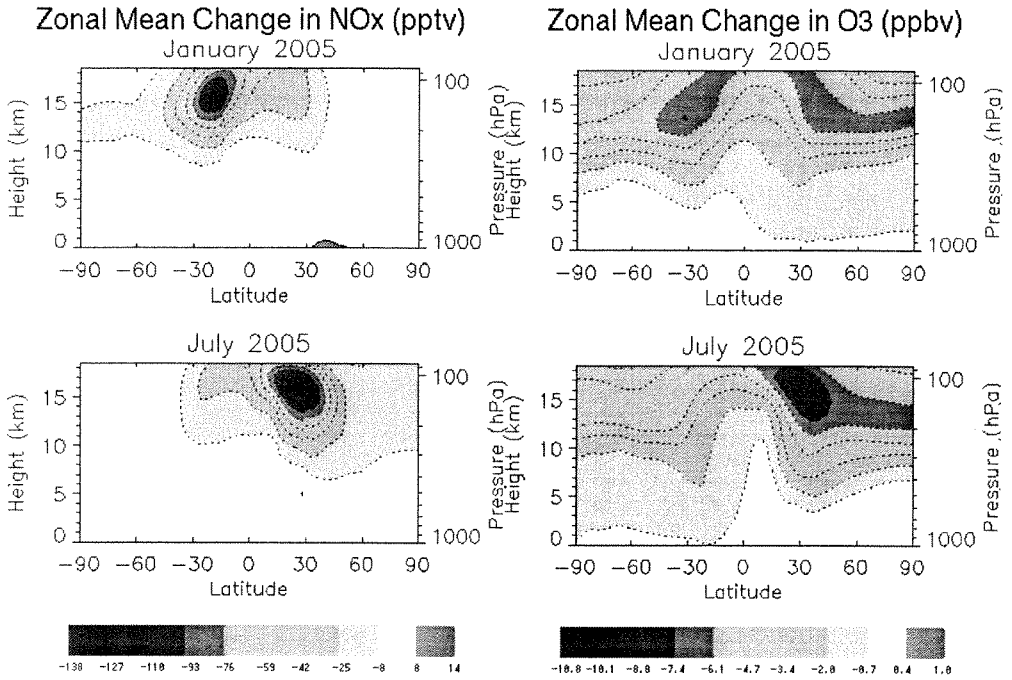

1053 Figure 13. Zonal mean change in NO_x (pptv) and O_3 (ppbv) in January and July resulting
1054 from using the lightning NO_x profiles in Figure 11 instead of the profiles from Pickering
1055 et al. [1998].

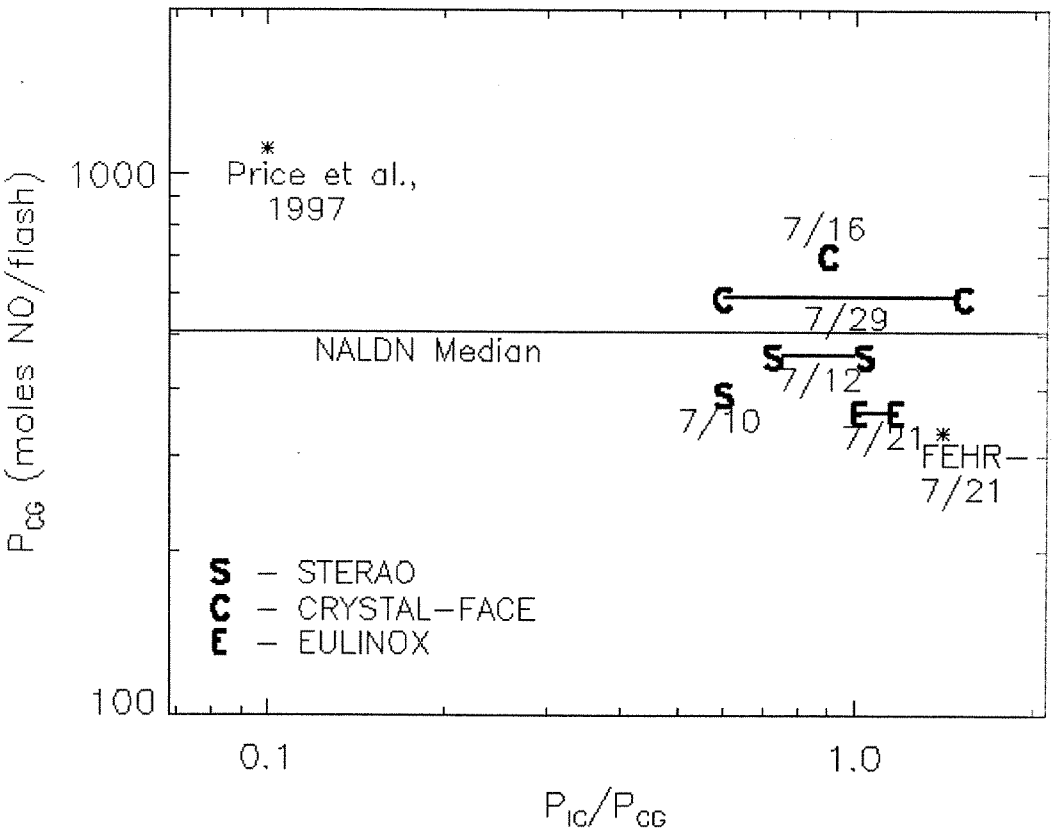

Figure 14. Estimated lightning NO_x production scenarios for the July 16 CRYSTAL-FACE (C, 7/16), July 29 CRYSTAL-FACE (C, 7/29), July 10 STERAO (S, 7/10), July 12 STERAO (S, 7/12), and July 21 EULINOX (E, 7/21) storms. The bars in the 7/29 CRYSTAL-FACE, 7/12 STERAO, and 7/21 EULINOX storms indicate the estimate uncertainty. The Price et al., [1997] and Fehr et al. [2004] production scenarios are indicated by asterisks, as is the estimated value of P_{CG} calculated assuming the NALDN median peak current from Orville et al. [2002].

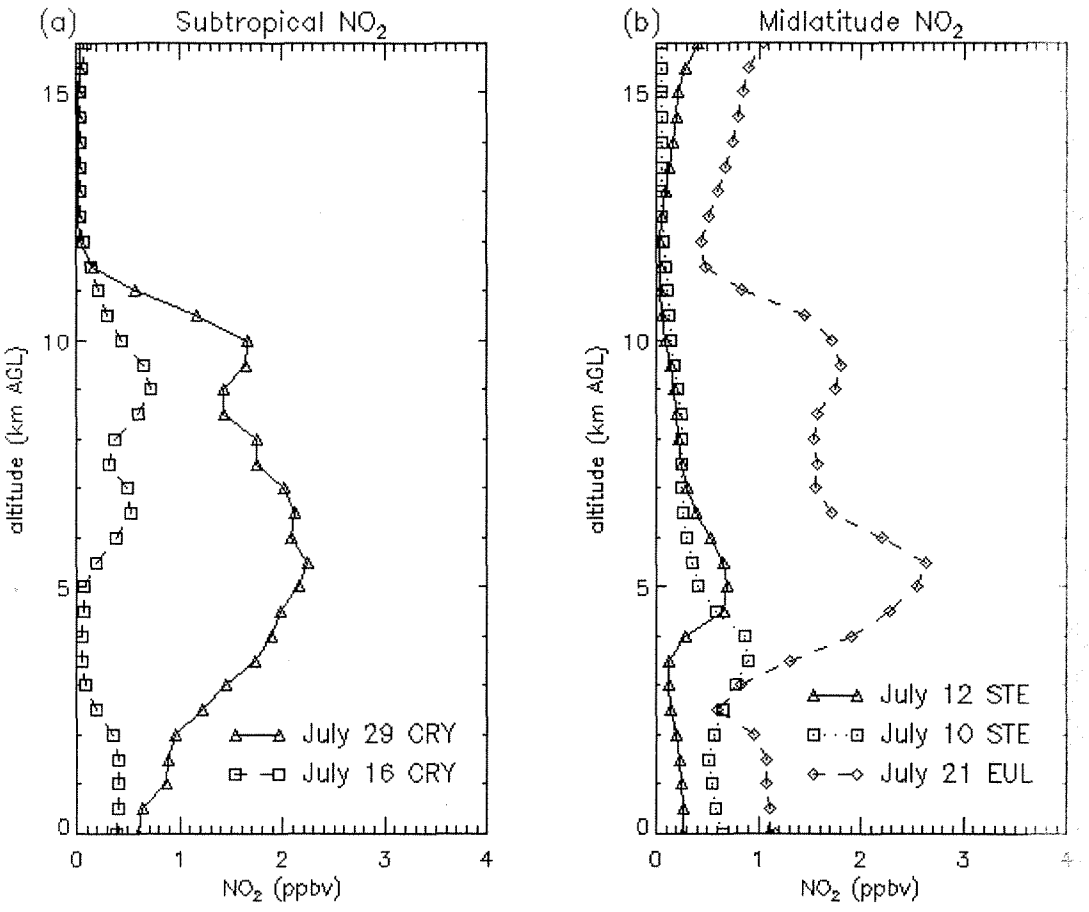

Figure 15. Average vertical profiles of NO_2 mixing ratio in the convective core region following simulated subtropical storms (a) and midlatitude storms (b).

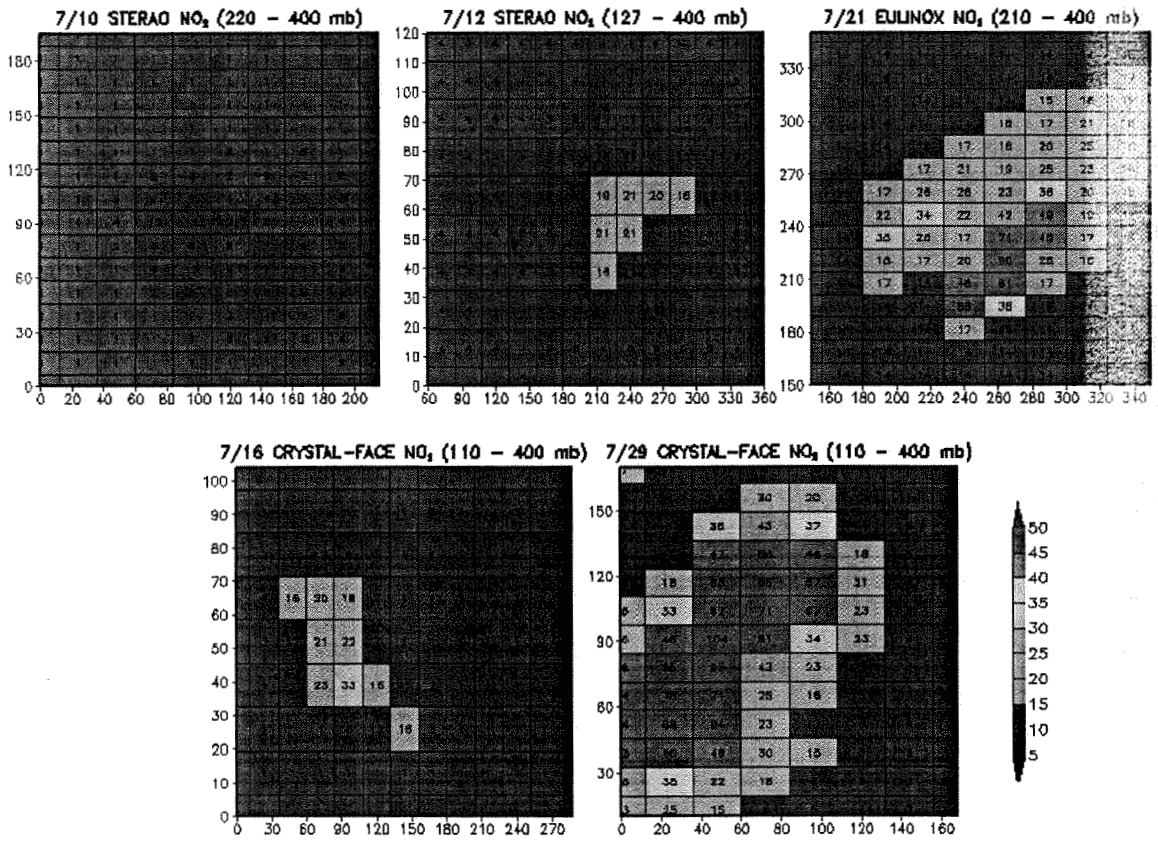

Figure 16. Partial NO_2 columns (10^{14} molecules cm^{-2}) from the tropopause to 400 hPa for CRYSTAL-FACE, STERAO, and EULINOX simulated thunderstorms.